Complex of an Active μ-Opioid Receptor with a Cyclic Peptide Agonist Modeled from Experimental Constraints†

Carol B. Fowler,‡,§ Irina D. Pogozheva,‡,§ Andrei L. Lomize,‡ Harry LeVine, III,|| and Henry I. Mosberg*,‡

Department of Medicinal Chemistry, University of Michigan, 428 Church Street, Ann Arbor, Michigan 48109-1065, and Department of Molecular and Cellular Biochemistry, Chandler School of Medicine and the Center on Aging, University of Kentucky, Lexington, Kentucky 40536

Received July 26, 2004; Revised Manuscript Received September 27, 2004

ABSTRACT: Site-directed mutagenesis and design of Zn^{2+}-binding centers have been used to determine a set of specific tertiary interactions between the μ-opioid receptor, a rhodopsin-like G protein-coupled receptor (GPCR), and its cyclic peptide agonist ligand, Tyr^1-c(S-Et-S)[D-Cys^2-Phe^3-D-Pen^4]NH_2 (JOM6). The binding affinity of the tetrapeptide is strongly dependent on the nature of its first and third residues and on substitutions at positions 213, 216, 237, 300, 315, and 318 of the μ-opioid receptor. His^1 and His^3 analogues of the ligand were able to form metal-binding complexes with the V300C and G213C/T315C receptor mutants, respectively. Direct contact of the Phe^3 residue of JOM6 with Gly^{213}, Asp^{216}, Thr^{315}, and Trp^{318} of the receptor was suggested by the binding affinities of His^3-, Nle^3-, Leu^3-, Aci^3-, Δ^EPhe^3-, and Δ^ZPhe^3-substituted peptides with the G213C/T315C, D216V, T315C, and W318L mutants. The improved binding affinity of the free carboxylate analogue of JOM6 for binding to the E229D mutant revealed an interaction between the C-terminal group of the peptide and Glu^{229} of the receptor. The experimental constraints that were obtained were applied for distance geometry modeling of the μ-receptor in complex with the tetrapeptide agonist ligand, JOM6. The active conformation of the opioid receptor was calculated using the crystal structure of "inactive" rhodopsin and published engineered and intrinsic metal-binding sites and disulfide bonds that allow or facilitate activation of GPCRs. Interhelical H-bonds existing in the μ-receptor were applied as additional distance constraints. The calculated model of the receptor−ligand complex can serve as a prototype of the active state for all rhodopsin-like GPCRs. It displays a strongly shifted transmembrane helix 6 (TM6) and reorientation of the conserved Trp^{293} residue in TM6 upon its interaction with the agonist. Importantly, the binding pockets of the active and inactive states are not identical, which implies distinct interaction modes of agonists and antagonists. In the active state, the binding pocket of the μ-receptor is complementary to the previously proposed receptor-bound conformation of JOM6.

The μ-, δ-, and κ-opioid and orphanin receptors are the rhodopsin-like G protein-coupled receptors (GPCRs)[1] involved in pain management and regulation of mood, reward, motivation, and response to stress (*1*). Opioid receptors are naturally activated by endogenous opioid peptides, but also can interact with exogenously administered opiates, some of which are addictive drugs of abuse. The activation of opioid receptors enables their transient association with Gi/o proteins (*2*), which triggers signal transduction through inhibition of adenylate cyclase, and regulation of ion channels and MAP kinases (*3*).

The binding of opioid ligands may have different functional outcomes. Opiates can act as agonists, antagonists, partial agonists, or inverse agonists. Opioid agonists can activate different transduction pathways, or have dissimilar profiles of dimerization, desensitization, endocytosis, up- and downregulation, or recycling of opioid receptors, which could induce tolerance, dependence, and addiction (*4*). The different efficacies of the drugs may be associated with the existence of multiple ligand-bound conformations of the receptors (*5*, *6*). Moreover, the entire activation may represent a sequence of conformational transitions between states with distinct cellular functions (*7*). The structural specifics of activation and receptor−ligand interactions can be understood only at the molecular level, for example, using X-ray crystallography of the receptor−agonist complexes. However, in the absence of such crystal structures, the problem can be addressed only by less direct methods, such as mutagenesis, labeling, cross-linking, analysis of structure−affinity relationships for series of agonists, or molecular modeling (*8*, *9*). Recently obtained 2.6−2.8 Å resolution crystallographic models of bovine rhodopsin provide a structural template for the study of other rhodopsin-like GPCRs (*10*, *11*). Four coordination sets of rhodopsin structures (PDB entries 1f88, 1hzx, 1l9h, and

† These studies were supported by Grant DA03910 from the National Institute on Drug Abuse (NIDA) and a NIDA predoctoral training grant.

* To whom correspondence should be addressed: Department of Medicinal Chemistry, University of Michigan, 428 Church St., Ann Arbor, MI 48109-1065. Phone: (734) 764-8117. Fax: (734) 763-5595. E-mail: him@umich.edu.

‡ University of Michigan.

§ These authors contributed equally to this work.

|| University of Kentucky.

[1] Abbreviations: EL, extracellular loop; GPCR, G protein-coupled receptor; TM, transmembrane helix; SEM, standard error of the mean.

10.1021/bi048413q CCC: $27.50
Published on Web 11/19/2004

1gzm) are currently available from the Protein Data Bank (*12*) and can be used for comparative modeling of rhodopsin-like receptors.

Unfortunately, two serious problems exist. First, the homology models are unreliable in the nonregular loop regions and may include significant misalignments, due to insertions of single residues in the middle of transmembrane (TM) helices. Such insertions ("α-aneurisms") are present in TM2 and TM5 of rhodopsin (*13*), but may not be a general feature for other GPCRs. Therefore, the design of spatial constraints, such as disulfide bonds or metal-binding centers, may be required for experimental verification and refinement of homology models (*14*, *15*). The second problem is related to the conformational rearrangement of the receptor during activation. The crystal structure of rhodopsin represents the inactive conformation in complex with the covalently bound inverse agonist, 11-*cis*-retinal. However, the active states of rhodopsin and other GPCRs have been shown to be different from the inactive conformations (*16*, *17*). Activation has been extensively studied using fluorescence, IR and UV spectroscopy, spin-labeling techniques, mutagenesis, the substituted cysteine accessibility method, disulfide cross-linking, design of metal-binding sites (*17*−*19*), and identification of constitutively active mutants (*20*). The accumulated data suggest that different rhodopsin-like GPCRs share a common active conformation (*21*), in which TM6 undergoes a significant rigid-body motion (*5*, *22*, *23*). During activation, the intracellular end of TM6 moves outward from TM3 (*22*, *24*) and TM7 (*25*, *26*), and toward TM5 (*5*), resulting in the opening of a cleft at the cytoplasmic surface of the α-bundle for binding of G proteins (*19*, *27*). Smaller motions of several other helices (1−3 and 7) have also been suggested (*23*, *28*−*31*). Some of the important structural data for the active state include the formation of disulfides between TM5 and TM6 in the ACM3 muscarinic receptor upon agonist binding (*32*), the existence of an intrinsic allosteric Zn^{2+}-binding site at the interface of TM5 and TM6 of the β_2-adrenergic receptor that facilitates agonist binding (*33*), and the engineering of an activating metal coordination center between TM3 and TM7 in β_2-adrenergic (*34*) and tachykinin receptors (*35*), and also between TM2 and TM3 of the MC4 melanocortin receptor (*36*).

In the study presented here, we use a combination of experimental and modeling methods to study binding of the μ-opioid receptor with its cyclic tetrapeptide ligand, Tyr-c(S-Et-S)[D-Cys-Phe-D-Pen]NH_2 (JOM6), an analogue in which cyclization is effected via an ethylene dithioether linkage involving the sulfurs of the D-Cys and D-Pen (penicillamine) side chains. This peptide is a μ-selective agonist with high binding affinity, functional potency, and efficacy (*37*, *38*). The conformation−activity relationships for related cyclic peptides have been extensively studied in our group. In particular, the pharmacological studies and conformational analysis of peptides with constrained Tyr^1 and Phe^3 residues (*39*−*42*) allowed deduction of the tentative receptor-bound conformation of JOM6[2] (*43*). Using this receptor-bound conformation, we have designed and examined Zn^{2+}-binding sites between His^1 and His^3 analogues of JOM6 and μ-receptor mutants with incorporated cysteine residues and have also examined the binding of several additional JOM6 analogues with different μ-receptor mutants. The data resulting from these experiments as well as other published information have been employed in distance geometry calculations to identify the active, agonist-bound conformation of the μ-opioid receptor in complex with JOM6.

EXPERIMENTAL PROCEDURES

Materials. The pCMV expression vector containing the coding sequence for the rat μ-opioid receptor (μ/pCMV) was obtained from H. Akil (University of Michigan). Pfu turbo DNA polymerase, DpnI restriction endonuclease, and XL1-blue supercompetent *Escherichia coli* cells were purchased from Stratagene. COS-1 (African green monkey kidney cell line, SV40 transformed) cells were obtained from the American Type Culture Collection (ATCC, catalog no. CRL-1650). Nucleotide primers, antibiotics, 1 M Tris-HCl buffer, Lipofectamine Plus reagent, and cell culture media were purchased from Life Technologies. [^{3}H]DAMGO was purchased from NEN. The 96-well Multiscreen-FC glass fiber filter plates (catalog no. MAFCN0B10) were purchased from Millipore. JOM6 and JOM6 analogues were prepared by standard solid phase methods as previously described for the synthesis of JOM6 (*37*). All other reagents were from Sigma-Aldrich unless otherwise indicated.

Site-Directed Mutagenesis. Single and double point mutations of the μ-opioid receptor were generated from the μ/pCMV expression vector using the QuikChange Mutagenesis Kit (Stratagene, La Jolla, CA). Each mutation was verified by DNA sequencing.

Cell Culture and Transfection. COS-1 cells were grown to 80% confluency in Dulbecco's modified Eagle's medium (high glucose) supplemented with 10% fetal bovine serum and incubated at 37 °C in 5% CO_2. Eight to ten micrograms per 75 cm^2 flask of the μ-opioid/pCMV wild-type and mutant plasmids were then transiently transfected into the cells using Lipofectamine Plus reagent (20 and 30 μL of Plus reagent and Lipofectamine, respectively, in a total volume of 300 μL of tranfection mixture per 6 mL of culture medium).

COS-1 Membrane Preparation. Whole membrane preparations for radioligand binding studies were prepared in a manner similar to established procedures (*44*). Briefly, 48 h after transfection, the COS-1 cells were scraped into 50 mM Tris-HCl (pH 7.4) containing 0.1 mg/mL PMSF (ice-cold) and homogenized using a Polytron homogenizer. Following centrifugation at 15000*g* for 30 min at 4 °C, the membranes were resuspended to a protein concentration of 0.2 mg/mL in the homogenization buffer. The concentration of the membrane protein was determined using the method of Bradford (*45*).

Radioligand Binding Assays. Forty to fifty micrograms of the COS-1 membrane protein preparations in 200 μL of 50 mM Tris-HCl (pH 7.4) was used for all binding studies. The membranes were incubated with 25 μL aliquots of [^{3}H]-DAMGO in 50 mM Tris-HCl (pH 7.4) in 96-well polypropylene microtiter plates. The radioligand (0.1−20 nM) was used for saturation binding studies. Competition binding

[2] Tyr^1: $\psi = 91°$, $\chi_1 = -178°$, and $\chi_2 = -102°$. DCys^2: $\varphi = 65°$, $\psi = 46°$, $\chi_1 = 170°$, $\chi_2 = 176°$, $\chi_3 = -110°$, and $\chi_4 = 60°$. Phe^3: $\varphi = -72°$, $\psi = -57°$, $\chi_1 = 177°$, and $\chi_2 = -102°$. DPen^4: $\varphi = 135°$, $\psi = -137°$, $\chi_1 = -55°$, $\chi_2 = 176°$, and $\chi_3 = -123°$ (after minimization of the peptide with CHARMm).

FIGURE 1: Sequence alignment of bovine rhodopsin and the rat μ-opioid receptor used for homology modeling of the μ-receptor. Underlined characters represent residues from α-helices, and underlined italic characters represent residues from β-strands. The most highly conserved GPCR residue in each TM (1.50, 2.50, 3.50, 4.50, 5.50, 6.50, and 7.50, in the nomenclature of ref *8*) is denoted with bold type and an asterisk. Mutation sites tested in this work are labeled in red. Natural and substituted (third row) residues involved in formations of the disulfide bonds and the Zn^{2+}-binding sites, consistent with receptor active conformations, are labeled in blue; residues participating in the alternative modes of cross-linking of TM5 and TM6 (in models 1−5) are denoted with italic type. Residues involved in formation of Zn^{2+}-binding sites between the μ-receptor and His^1 or His^3 analogue of JOM6 are labeled in green.

assays were carried out in the presence of 2 nM [^{3}H]DAMGO and 0.1 nM to 30 μM peptide ligands. Nonspecific binding was assessed in the presence of 2 μM unlabeled Naloxone. After being incubated for 1.5 h at room temperature, the samples were transferred to 96-well glass fiber filter plates, filtered, and washed with 2 × 200 μL of ice-cold 50 mM Tris-HCl (pH 7.4). Filter plates were saturated with 100 μL of Beckman Ready Gel and counted using a Wallac Trilux1450 scintillation counter.

Data Analysis. The saturation binding results were analyzed, and K_D and B_{max} values for the wild-type and receptor mutants were determined using the LIGAND module of RADLIG (Biosoft, Ferguson, MO). Saturation binding experiments were carried out in duplicate, and K_D values are expressed in nanomolar ± the standard error of the mean (SEM). Competition binding assays were analyzed using SigmaPlot 7.0 (SPSS Science, Chicago, IL). All competition binding curves were fit by nonlinear regression, and IC_{50} values were determined from the fitted curve. Average IC_{50} values reported for competition assays are ± SEM based on two or more independent experiments, each carried out in duplicate. IC_{50} values were converted to K_i values using the Cheng−Prusoff correction (*46*), where $K_i = IC_{50}/1 + [\text{radioligand}]/K_D(\text{radioligand})$.

Distance Geometry Calculations of the Receptor−Ligand Complex. The receptor−agonist complex was calculated using DIANA (*47*), QUANTA (Accelrys), and our in-house software, as described previously (*15*, *48*−*50*). Several types of constraints were applied. First, the spatial positions of all transmembrane helices, except TM6, were restrained as in the rhodopsin template (PDB entry 1gzm) by using the corresponding $C^\beta-C^\beta$ distances, with deviations of 1 Å, as upper distance constraints. This allows arbitrary movements of TM6 and small spatial adjustments of all other helices during the calculations. The sequence alignment of the μ-receptor and rhodopsin (Figure 1) was verified previously using intrinsic and engineered Zn^{2+}-binding centers and other data (*15*). It assumes the absence of the α-aneurism in TM2 observed in rhodopsin but conservation of the rhodopsin-like β-hairpin in the second extracellular loop (EL2) of opioid receptors.

Second, we included a set of experimental constraints: (1) two engineered Zn^{2+}-binding sites between the μ-receptor and JOM6 analogues, which were identified in this work; (2) a conserved S−S bond (140−217[3]) present in the native μ-receptor between TM3 and EL2 (*51*); (3) five engineered disulfide bridges that are permissive for the active conformation of rhodopsin and can be formed between TM1 and helix 8 (96−346), TM3 and TM5 (170−254, 166−254, and 169−254), or TM5 and TM6 (233−304) (*52*, *53*); (4) two designed activating Zn^{2+}-binding centers [one between TM2 and TM3 (Q124E and V143H) from the MC4 melanocortin receptor

[3] Rat μ-receptor residue numbering.

(*36*) and another involving TM3 and TM7 (I322C and Asp^{147}) of β_2-adrenergic or tachykinin receptors (*34*, *35*)]; and (5) two H-bond constraints derived from constitutively active mutants of rhodopsin (Arg^{165}-V285N) (*25*) and the δ-opioid receptor (Asp^{147}-Y326H) (*54*). In addition, we tested five alternative cross-linking constraints between TM5 and TM6: four disulfide bridges, whose formation is facilitated by agonist binding to the ACM3 muscarinic receptor (256−279, 256−280, 256−281, and 256−282) (*32*) or an allosteric Zn^{2+}-binding center that enhances binding of the agonist to the β_2-adrenergic receptor (R258E, D272C, and R276H; *33*). These constraints were incorporated by replacing the corresponding residues with Cys, His, Glu, or Asn in the μ-opioid receptor sequence (Figure 1; see Table 5 in the Results). The upper limits for constraints were chosen to be 2.04, 3.05, and 4.20 Å for $S^{\gamma}-S^{\gamma}$, $C^{\beta}-S^{\gamma}$, and $C^{\beta}-C^{\beta}$ distances, respectively, in disulfide bonds and 3.5 Å for $O^{\delta/\epsilon}-N^{\epsilon}$ and $O^{\delta/\epsilon}-S^{\gamma}$ distances in metal-binding centers involving His, Cys, Asp, or Glu residues.

Third, we included an evolving system of hydrogen bonding constraints that was iteratively refined during the calculations, as described previously (*15*, *48*). These H-bonds were incorporated between transmembrane α-helices and between the receptor and ligand (see Table 6 in the Results). The upper limits were 1.9 Å for H···O, 2.9 Å for O···O and N···O, and 3.6 Å for O···S H-bonds. Finally, the dihedral angles in α-helices were constrained ($\varphi = -70°$ to $-50°$, $\psi = -50°$ to $-30°$). Most of the side chain conformers (χ angles) were "traced" as in the rhodopsin template, while others were adjusted during the iterative distance geometry refinement. The allowed deviations for the χ angles were ±30°. The optimization protocol and weighting factors were described previously (*48*).

Importantly, the cyclic peptide was directly included in the distance geometry calculations. Thus, a separate docking procedure was not required. The nonstandard D-Cys-S-CH3 and D-Pen-S-CH3 residues were incorporated into the DIANA library. The dihedral angles of JOM6 were restrained as in the lowest-energy conformer of the peptide (*43*). This conformer has been suggested to be bioactive on the basis of comparisons with a more rigid μ-selective peptide Tyr-c[D-Cys-Δ^{E}Phe-D-Pen]NH_2 (*41*, *42*). The torsion angles within the cycle were constrained, with an allowed deviation of ±30°, for D-Cys^2 ($\varphi_2 = 90°$, $\psi_2 = 30°$, $\chi_1 = 180°$, and $\chi_2 = 180°$), Phe^3 ($\varphi_3 = -70°$ and $\psi_2 = -40°$), and D-Pen^4 ($\varphi_4 = 120°$, $\psi_4 = -150°$, $\chi_1 = -60°$, and $\chi_2 = 180°$) residues. The side chains of Tyr^1 and Phe^3 of JOM6 were fixed in the *trans* orientation ($\chi_1 = 180°$ and $\chi_2 = 90°$), in agreement with the binding requirements for the cyclic peptides with conformationally restrained first and third residues (*39*−*41*). Attempts to restrict the torsion angles in alternative, higher-energy conformers of JOM6 (*43*) led to structures of the complexes with a higher target function and forbidden torsion angles. Thus, the alternative conformers of JOM6 did not fit the binding pocket.

The model of the receptor−ligand complex was generated in two steps. First, the calculations were conducted using the modified amino acid sequences of the receptor and peptide ligand to combine the experimental active state constraints from different GPCRs. This was done with five alternative versions of constraints between TM5 and TM6, from which the final model was selected, as described in the Results. Second, the calculations were repeated with native sequences of the receptor and ligand, and using $C^{\beta}-C^{\beta}$ constraints taken from the model with the lowest target function obtained in the previous step, instead of experimental constraints. The allowed deviation for the $C^{\beta}-C^{\beta}$ distances was taken to be ±0.5 Å. The rmsds of C^{α} atoms within the sets of 10 best conformers generated with DIANA in both steps were <0.8 Å. Similar calculations were also repeated for the ligand-free receptor. The rmsd between the ligand-free and ligand-bound active conformations of the μ-receptor was 0.5−0.8 Å for 291 C^{α} atoms.

The complexes of the μ-receptor with the Tyr^1 and Phe^3 analogues of JOM6 were generated by substituting the corresponding residues in the peptide, followed by (a) adjustment of side chain rotamers in the binding pocket to minimize clashes, (b) application of the standard docking procedure (DOCK) from QUANTA, and (c) energy minimization (100 iterations) of the complex with the CHARMm force field (*55*, *56*) using a dielectric constant ϵ of 10 and the adopted-basis Newton−Raphson method.

RESULTS

In the experiments described below, we identified residues of the μ-receptor that are in direct contact with specific functional groups of the peptide ligand. This was accomplished by reciprocal modifications of JOM6 and μ-receptor residues. Several lower-affinity JOM6 analogues with modified Tyr^1, Phe^3, or C-terminal carboxamide groups were prepared and probed with different μ-receptor mutants to find "rescue" mutations that could restore the ligand binding affinity. An important element of this strategy was the design of a metal coordination site between receptor and ligand residues that increased the binding affinity for JOM6 analogues in the presence of Zn^{2+}. Importantly, the corresponding mutations did not significantly alter the natural binding pocket, as was evident from the high affinity of the parent peptide. The rhodopsin-based model of the μ-opioid receptor (*15*) was used for planning the mutation sites. This model has a narrow binding cavity between TM helices 3−7 and extracellular loop 2, whose size is sufficient to accommodate the cyclic or linear opioid peptides or alkaloids. The common tyramine (Tyr^1) portion of the opioid ligands can occupy the bottom of the cavity between Asp^{147} (TM3) and His^{297} (TM6) (*15*, *49*, *57*). However, such an arrangement of JOM6 must be verified and refined in the context of the active conformation. Moreover, the identification of specific contacts between the receptor and ligand residues was essential for subsequent automated docking of the peptide by distance geometry during modeling of the ligand−receptor complex.

Interactions of Tyr^1 with Phe^{237} (TM5) and Val^{300} (TM6). His^1 of the JOM6 analogue together with His^{297} and Cys^{300} residues of the μ-receptor can form a metal-binding center in the V300C mutant. To identify the contacts between Tyr^1 of JOM6 and the μ-receptor, we designed and constructed a metal-binding cluster between the ligand and receptor. To do so, Tyr^1 of the ligand and several surrounding residues of the receptor (N230, F237, and V300) were substituted with histidines or cysteines. The results of competition binding assays, against [^{3}H]DAMGO, of the His^1 analogue of JOM6 are summarized in Table 1. The affinity of the His^1

Table 1: Influence of Addition of Zn^{2+} on the Competition of His^1-JOM6 with [^{3}H]DAMGO for Binding with the μ-Opioid Receptor and Its Mutants[a]

	DAMGO	His^1-JOM6					
	0 μM Zn^{2+}	0 μM Zn^{2+}		20 μM Zn^{2+}		30 μM Zn^{2+}	
μ-receptor	K_D (nM)	IC_{50} (nM)	K_i (nM)	IC_{50} (nM)	K_i (nM)	IC_{50} (nM)	K_i (nM)
wild type	1.1 ± 0.33[b]	1500 ± 80 (3)[c]	530 ± 30	1500 ± 100 (3)	530 ± 40	1500 ± 100 (2)	530 ± 40
N230H	1.0 ± 0.11	1500 ± 120 (2)	500 ± 40	1320 ± 260 (2)	440 ± 86	1300 ± 50 (2)	433 ± 17
V300C	2.5 ± 0.89	150 ± 10 (4)	80 ± 6.0	50 ± 2.0 (3)	30 ± 2.0	50 ± 2.0 (3)	27 ± 6.0
F237C	3.8 ± 1.3	5000 ± 150 (2)	3300 ± 100	2000 ± 120 (2)	1300 ± 80	nd[d]	nd[d]

[a] Competition assays were carried out in the presence of 2 nM [^{3}H]DAMGO and 0.1 nM to 30 μM peptide ligands. Nonspecific binding was assessed in the presence of 2 μM unlabeled naloxone. Single concentrations of Zn^{2+} were added to each assay as indicated. Values are ±SEM based on two or more independent experiments, each carried out in duplicate. The number of independent experiments is indicated in parentheses. IC_{50} values were converted to K_i values using the Cheng−Prusoff correction (*46*). [b] Binding of [^{3}H]DAMGO to the wild-type μ-receptor was not significantly affected by Zn^{2+} at concentrations up to 30 μM. [c] The K_i for the parent peptide, JOM6, at the wild-type μ-receptor in the absence of Zn^{2+} was 0.32 ± 0.1 nM (see Tables 2−4). [d] Not determined due to a reduced level of binding of [^{3}H]DAMGO to this mutant at 30 μM Zn^{2+}.

Table 2: Influence of Phe^3 Substitution on the Binding of JOM6 Analogues to the μ-Opioid Receptor and Its Mutants[a]

	wild type[b]		T315C[c]		G213C/T315C[d]	
	IC_{50} (nM)	K_i (nM)	IC_{50} (nM)	K_i (nM)	IC_{50} (nM)	K_i (nM)
JOM6	0.9 ± 0.04 (3)	0.32 ± 0.01	0.9 ± 0.1 (3)	0.5 ± 0.06	0.76 ± 0.1 (2)	0.1 ± 0.01
His^3-JOM6	300 ± 30 (3)	106 ± 11	60 ± 5.0 (3)	34 ± 2.8	50 ± 3.0 (4)	6.5 ± 0.9
Nle^3-JOM6	30 ± 2.3 (2)	11 ± 0.8	30 ± 1.9 (2)	17 ± 1.1	30 ± 1.5 (2)	3.9 ± 0.2
Leu^3-JOM6	1000 ± 97 (2)	355 ± 34	3000 ± 450 (2)	1700 ± 250	1000 ± 55 (2)	130 ± 7.2
Aci^3-JOM6	60 ± 3.6 (3)	21 ± 1.3	10 ± 0.8 (3)	5.6 ± 0.4	nd[e]	nd[e]

[a] Competition assays were carried out as described in the legend of Table 1. Aci, 2-aminoindan-2-carboxylic acid; Nle, norleucine. [b] With DAMGO (K_D = 1.1 ± 0.33 nM). [c] With DAMGO (K_D = 2.6 ± 1.3 nM). [d] With DAMGO (K_D = 0.3 ± 0.1 nM). [e] Not determined.

analogue for the wild-type receptor was reduced greatly (K_i = 530 nM) in comparison with the parent Tyr^1 peptide [K_i = 0.32 nM (*15*)]. However, the binding was partially restored in the V300C mutant, indicating a stabilizing interaction between His^1 and Cys^{300} (~7-fold decrease of K_i in comparison with that of the wild type). Moreover, the ligand affinity was increased further in the presence of Zn^{2+} ions for this mutant (K_i = 27−30 nM). An inspection of the approximate model shows that, in addition to Cys^{300} and His^1, the corresponding metal binding center can also include the His^{297} residue, which is naturally present in TM6. Unlike the V300C replacement, the N230H substitution did not change the His^1-JOM6 binding in the presence or absence of zinc. The affinity of His^1-JOM6 for the F237C mutant was greatly reduced (K_i = 3300 nM) and zinc-sensitive (Table 1). The altered sensitivity indicates that His^1 of the tetrapeptide is proximal to Phe^{237} but not to Asn^{230} in TM5 of the μ-receptor.

When these experiments are interpreted, it is important to realize that Zn^{2+} coordination sites can be formed either between the receptor and ligand or between several residues of the receptor itself. Indeed, Zn^{2+} ions can bind to His^{297}-V300C or His^{297}-F237H clusters of the μ-opioid receptor, which inhibits its association with naloxone or DAMGO with an $IC_{50}(Zn^{2+})$ of 20 or 10 μM, respectively (*15*). However, the His^1 analogue, unlike the parent peptide, had a higher affinity for the V300C mutant, especially at increased concentrations of Zn^{2+}, which suggests the formation of the His^1-Cys^{300}-His^{297} metal coordination center.

Interactions of Phe^3 of JOM6 with Residues 213 and 315 in the Second (EL2) and Third (EL3) Extracellular Loops, Respectively. These interactions were probed using several Phe^3-substituted analogues of JOM6, which all have binding affinities lower than that of the parent peptide (Table 2). The affinity of the His^3 analogue was low (K_i ~ 106 nM), but was significantly increased in the single T315C (EL3) and T315C/G213C (EL3/EL2) double mutants (K_i = 34 and 6.5 nM, respectively). Binding of His^3-JOM6 to the T315C mutant appeared to be zinc-insensitive, but the double mutant demonstrated an ~2-fold better affinity in the presence of 20 μM Zn^{2+} (not shown). Thus, His^3 of the JOM6 analogue and the Cys^{213} and Cys^{315} residues of the μ-receptor probably form a metal binding site. The binding affinity of Aci^3-JOM6 was also increased in the T315C mutant, which can be explained by a stabilizing noncovalent interaction between Aci^3 and Cys^{315}. Both Nle^3 and Leu^3 analogues bind better to the double than to the single cysteine mutant; however, the replacement by Nle^3 or Leu^3 strongly inhibits the binding in all mutant and wild-type receptors. All these results indicate interactions of residues 213 and 315 in μ-opioid receptors with Phe^3 of JOM6.

Interaction of the Phe^3 Residue with Trp^{318} in TM7. The $\Delta^E Phe^3$ and $\Delta^Z Phe^3$ analogues of JOM6 (Table 3) have the side chain of Phe^3 constrained in *trans* and *gauche*-like orientations, respectively. Comparison of their binding affinities in Table 3 demonstrates that the μ-opioid receptor has a strong preference for the Δ^E-Phe^3 analogue of JOM6 (K_i = 2.9 nM for $\Delta^E Phe^3$-JOM6 compared with 138 nM for $\Delta^Z Phe^3$-JOM6), consistent with our previous observation (*43*). As discussed previously (*43*), these results indicate that the Phe^3 side chain of JOM6 adopts a *trans* orientation at the μ-receptor binding site.

In the model of the inactive μ-receptor (*15*), Phe^3 of JOM6 is close to Trp^{318} (TM7), a residue that is important for selective binding of peptide ligands (*58*−*60*). To test whether the interaction between Phe^3 of JOM6 and Trp^{318} of the μ-receptor is critical for the observed requirement for the *trans* orientation of the Phe^3 side chain, we compared the binding of $\Delta^E Phe^3$-JOM6 and $\Delta^Z Phe^3$-JOM6 to the wild-type μ-receptor and the W318L mutant (substitution with

Table 3: Influence of the Restricted Ligand Side Chain Conformation on the Binding of Phe[3] Analogues of JOM6 to the μ-Opioid Receptor and Its Mutants[a]

	[^{3}H]DAMGO	JOM6		Δ^EPhe JOM6		Δ^ZPhe JOM6	
μ-receptor	K_D (nM)	IC_{50} (nM)	K_i (nM)	IC_{50} (nM)	K_i (nM)	IC_{50} (nM)	K_i (nM)
wild type	1.1 ± 0.33	0.9 ± 0.08 (4)	0.32 ± 0.01	8.3 ± 0.3 (3)	2.9 ± 0.1	395 ± 30 (3)	138 ± 10
W318L	0.94 ± 0.3	3.0 ± 0.18 (3)	0.96 ± 0.06	1000 ± 4 (3)	319 ± 15	395 ± 20 (3)	96 ± 6.7
D216V	0.9 ± 0.6	0.2 ± 0.03 (3)	0.06 ± 0.01	4.0 ± 0.3 (3)	1.2 ± 0.11	200 ± 20 (2)	64 ± 6.2
S214A/D216V	1.3 ± 0.7	0.3 ± 0.02 (2)	0.11 ± 0.01	nd[b]	nd[b]	300 ± 21 (2)	118 ± 8.0

[a] Competition assays were performed as described in the legend of Table 1. [b] Not determined.

Table 4: Influence of the Ligand C-Terminal Group on the Binding of JOM6 Analogues to the μ-Opioid Receptor and Its Mutants[a]

	[^{3}H]DAMGO	JOM6		JOM18		
μ-receptor	K_D (nM)	IC_{50} (nM)	K_i (nM)	IC_{50} (nM)	K_i (nM)	JOM18/JOM6 K_i ratio
wild type	1.1 ± 0.33	0.9 ± 0.04 (3)	0.32 ± 0.01	4000 ± 320 (3)	1400 ± 112	4400
E229D	1.4 ± 0.39	5.5 ± 0.66 (3)	2.2 ± 0.27	404 ± 4.0 (3)	165 ± 1.6	73
E229D/E310R	3.3 ± 1.3	0.63 ± 0.6 (2)	0.39 ± 0.37	475 ± 25 (3)	289 ± 15	753

[a] Competition assays were performed as described in the legend of Table 1.

the residue present in the δ-receptor). As summarized in Table 3, the W318L mutant retained affinity for the parent JOM6 peptide (K_i = 0.96 nM, compared to 0.32 nM for the wild type), which indicates no significant structural changes in the binding pocket. However, the μ-selective Δ^EPhe^3-JOM6 analogue exhibited a 125-fold decreased binding affinity for W318L compared to that of the wild-type receptor (K_i = 319 and 2.9 nM, respectively). This suggests the presence of some unfavorable interactions (probably interatomic overlaps) between the constrained side chain of Δ^EPhe^3 and the W318L residue. On the other hand, the binding of the Δ^ZPhe^3 analogue to the wild-type μ-receptor and the binding to the W318L mutant were similar. These results suggest interaction between Trp^{318} and the *trans* conformer of Phe^3 in the bound peptide, although the W318L substitution alone was insufficient for producing binding affinities typical for the δ-opioid receptor.

Interaction of the JOM6 C-Terminal Carboxamide with Glu^{229} in TM5. The pharmacological evaluation of opioid peptides confirmed that the C-terminal free carboxyl group of peptides favored δ-selectivity, while amidation of C-terminus increased μ-selectivity (*57*). It was suggested that a negatively charged residue of the μ-receptor could have unfavorable ionic interaction with the free carboxyl group of the ligand. Examination of the model of the inactive μ-opioid receptor (*15*) suggested the presence of two acidic residues in the extracellular part of the μ-receptor, Glu^{229} (TM5) and Glu^{310} (EL3). To probe whether these negatively charged residues are responsible for μ-selective interaction with the C-terminal carboxamide of tetrapeptides, we mutated Glu^{229} to Asp and Glu^{310} to Arg (residues present in the δ-receptor) and compared the binding affinities of the corresponding mutants to those of peptides with amidated and free C-terminal carboxylates, JOM6 and JOM18, respectively (Table 4).

As summarized in Table 4, the replacement of the C-terminal carboxamide with an ionizable carboxyl group reduced the peptide affinity for the wild-type μ-receptor by ~4400-fold (K_i = 1400 and 0.32 nM for JOM18 and JOM6, respectively). However, the affinity of the modified peptide was partially restored (~10-fold increase) in the E229D mutant, while the affinity of JOM6 decreased ~6-fold, resulting in an increase in the relative affinity of JOM18 by ~60-fold. Thus, the low affinity of the carboxylated peptide (JOM18) is likely due, in part, to electrostatic repulsion of the charged C-terminus in the peptide and Glu^{229} in the μ-receptor, a repulsion that is weakened in the E229D mutant because of the shorter side chain of Asp versus Glu. On the other hand, the E229D/E310R double mutant has no additional influence on ligand affinity, suggesting that the Glu^{310} residue does not interact with the C-terminus of the JOM6 ligand.

Modeling of JOM6 in Complex with the Active Conformation of the μ-Receptor. The active conformation of the rat μ-opioid receptor in complex with JOM6 was calculated by distance geometry, as described in Experimental Procedures. The shifts of α-helices during activation were reproduced by using a set of receptor-specific H-bonds and experimental cross-linking constraints, permissive for activation of GPCRs (Tables 5 and 6). Importantly, a majority of these constraints are generally consistent with the model of the inactive state and therefore only slightly modulate the positions of the helices involved. By contrast, four disulfide bonds or a zinc binding cluster between the intracellular domains of helices 5 and 6 was inconsistent with the inactive structure, and their incorporation caused significant movement of TM6. These latter structural constraints are especially important, because they promote activation of receptors: binding of Zn^{2+} to the native allosteric center that involves Glu (5.64),[4] Cys (6.27), and His (6.31) residues was shown to improve the affinity for the agonist in the β_2-adrenergic receptor (*33*), while the formation of disulfide bonds between cysteines in TM5 (5.62) and TM6 (either 6.34, 6.35, 6.36, or 6.37) was strongly coupled with the binding of the agonist to the ACM3 muscarinic receptor (*32*). These disulfide bonds and the metal binding center are structurally incompatible with each other. Therefore, they were introduced independently in five different calculations.

The five resulting models of the active state vary in the positions of TM6 with maximal deviations for the residues at the cytoplasmic end of TM6 ranging from 7 (model 2) to 11 Å (model 4) relative to the model of the inactive conformation. These models were tested for consistency with

[4] The residue numbering scheme uses the generic system of Ballesteros and Weinstein (*8*).

Table 5: H-Bonds Applied as Distance Constraints (2.9 Å) for Modeling of the Active Conformation of the Rat μ-Opioid Receptor Models

residues		atoms	location	residues		atoms	location
D[a]	A[a]	D−A	D−A	D	A	D−A	D−A
Ser[64]	Thr[67]	Oγ−Oγ1	TM1−TM1	Asn[188]	Ala[184]	Nδ2−O	TM4−TM4
Thr[70]	Val[66]	Oγ1−O	TM1−TM1	Asn[191]	Thr[157]	Nδ2−Oγ1	TM4−TM3
Tyr[75]	Q124E[b]	Oη−Oϵ2	TM1−TM2	Trp[192]	Asn[109]	Nϵ1−Oδ1	TM4−TM2
Ser[76]	Met[72]	Oγ−O	TM2−TM2	Ser[195]	Asn[191]	Oγ−O	TM4−TM4
Asn[86]	Gly[82]	Nδ1−O	TM2−TM2	Thr[207]	Tyr[227]	Oγ1−O	EL2−EL2
Asn[86]	Ser[329]	Nδ2−O	TM1−TM7	Tyr[210]	Gly[199]	Oη−O	EL2−TM4
Arg[95]	Glu[349]	Nη2−Oϵ1	TM1−hel8	Arg[211]	Ser[222]	Nη2−Oγ	EL2−EL2
Tyr[96]	Glu[349]	Oη−Oϵ1	IL1−hel8	Gln[212]	Gly[213]	Nϵ2−O	EL2−EL2
Lys[100]	Ile[93]	Nζ−O	IL1−TM1	Gln[212]	Gly[214]	Nϵ2−O	EL2−EL2
Lys[100]	Tyr[96]	Nζ−O	IL1−TM1	Thr[218]	Tyr[148]	Oγ1−Oη	EL2−TM3
Thr[101]	Asn[104]	Oγ1−Oδ1	IL1−TM2	Thr[220]	Glu[229]	Oγ1−Oϵ1	EL2−TM5
Tyr[106]	Asp[164]	Oη−Oδ1	TM2−TM3	His[223]	Glu[310]	Nϵ2−Oϵ1	EL2−EL3
Asn[109]	Thr[157]	Nδ2−Oγ1	TM2−TM3	Thr[225]	Ser[222]	Oγ1−O	EL2−EL2
Thr[118]	Asp[114]	Oγ1−O	TM2−TM2	Thr[249]	Val[245]	Oγ1−O	TM5−TM5
Ser[119]	Ala[115]	Oγ−O	TM2−TM2	Ser[266]	Arg[263]	Oγ−O	IL3−TM5
Thr[120]	Ala[117]	Oγ1−O	TM2−TM2	Arg[276]	Asp[272]	Nη2−Oδ2	TM6−TM6
Ser[125]	Leu[121]	Oγ−O	TM2−TM2	V285N[c]	Tyr[252]	Nδ2−Oη	TM6−TM5
Tyr[128]	Q124E[b]	Oη−Oϵ2	TM2−TM2	Cys[292]	Asn[328]	Sγ−Oδ1	TM6−TM7
Asn[137]	Tyr[210]	Nδ2−O	TM3−EL2	Thr[294]	Ile[290]	Oγ1−O	TM6−TM6
Asn[150]	Ala[113]	Nδ2−O	TM3−TM2	Tyr[299]	Ser[317]	Oη−Oγ	TM6−TM6
Asn[150]	Asp[114]	Nδ2−Oδ1	TM3−TM2	Thr[307]	Lys[303]	Oγ1−O	TM6−TM6
Ser[154]	Asn[150]	Oγ−O	TM3−TM3	His[319]	Asp[216]	Nδ1−Oδ2	TM7−EL2
Thr[160]	Phe[156]	Oγ1−O	TM3−TM3	Asn[328]	Ser[154]	Nδ2−Oγ	TM7−TM3
Ser[162]	Leu[158]	Oγ−O	TM3−TM3	Ser[329]	Asn[150]	Oγ−Oδ1	TM7−TM3
Arg[165]	Tyr[336]	Nη1−Oη	TM3−TM7	Asn[332]	Ser[154]	Nδ2−Oγ	TM7−TM3
Arg[165]	Tyr[252]	Nη2−Oη	TM3−TM5	Asn[332]	Asn[328]	Nδ2−O	TM7−TM7
Arg[165]	V285N[c]	Nη2−Oδ1	TM3−TM6	Asn[342]	Asp[340]	N−Oδ1	hel8−hel8
Asn[188]	Ile[105]	Nδ2−O	TM8−TM2	Lys[344]	Phe[338]	Nζ−O	hel8−TM7
Asn[183]	Tyr[106]	Nδ2−Oη	TM4−TM2	Arg[345]	Glu[341]	Nη1−Oϵ1	hel8−hel8

[a] H-donors are marked as D and H-acceptors as A. [b] The Q124E substitution was introduced to form a Zn^{2+}-binding site between TM2 and -3 (*36*). [c] The V285N substitution leads to the constitutive activation of GPCR (*5*).

Table 6: Experimental Constraints Applied for Modeling of the Active Conformation of the Rat μ-Opioid Receptor Models

residues		atoms (distances, Å)	location
		S−S Bonds in the Receptor	
Y96C	Cys[346]	Cβ−Cβ (4.2), Cβ−Sγ (3.05), Sγ−Sγ (2.04)	TM1−hel8
Cys[140]	Cys[217]	Cβ−Cβ (4.2), Cβ−Sγ (3.05), Sγ−Sγ (2.04)	TM3−EL2
Cys[170]	L254C	Cβ−Cβ (4.2), Cβ−Sγ (3.05), Sγ−Sγ (2.04)	TM3−TM5
K233C	A304C	Cβ−Cβ (4.2), Cβ−Sγ (3.05), Sγ−Sγ (2.04)	TM3−TM5
Tyr[166]	L254C	Cβ−Cβ (6.0)	TM3−TM5
Val[169]	L254C	Cβ−Cβ (6.0)	TM3−TM5
I256C	V282C (5)[a]	Cβ−Cβ (4.2), Cβ−Sγ (3.05), Sγ−Sγ (2.04)	TM5−TM6
I256C	T279C (1)[a]	Cβ−Cβ (4.2), Cβ−Sγ (3.05), Sγ−Sγ (2.04)	TM5−TM6
I256C	R280C (3)[a]	Cβ−Cβ (4.2), Cβ−Sγ (3.05), Sγ−Sγ (2.04)	TM5−TM6
I256C	M281C (4)[a]	Cβ−Cβ (4.2), Cβ−Sγ (3.05), Sγ−Sγ (2.04)	TM5−TM6
		Zn^{2+}-Binding Sites in the Receptor	
Q124E	V143H	Oϵ1−Nδ1 (3.5)	TM2−TM3
Asp[147]	I322C	Oδ1−Sγ (3.5)	TM3−TM7
Asp[147]	Y326H	Oδ1−Nϵ2 (3.5)	TM3−TM7
R258E	D272C (2)[a]	Oϵ1−Sγ (3.5)	TM5−TM6
R258E	R276H (2)[a]	Oϵ1−Nϵ2 (3.5)	TM5−TM6
D272C	R276H (2)[a]	Sγ−Nϵ2 (3.5)	TM5−TM6
		Zn^{2+}-Binding Sites and H-Bonds between the Receptor and His[1],His[3]-JOM6	
His[297]	Y1H	Nϵ2−Nϵ2 (3.5)	TM6−ligand
V300C	Y1H	Sγ−Nϵ2 (3.5)	TM6−ligand
His[297]	V300C	Nϵ2−Sγ (3.5)	TM6−TM6
G213C	Y3H	Sγ−Nϵ2 (3.5)	EL2−ligand
T315C	Y3H	Sγ−Nϵ2 (3.5)	EL3−ligand
G213C	T315C	Sγ−Sγ (3.5)	EL2−EL3
Asp[147]	Y1H	Oδ1−N (2.9)	TM3−ligand
Glu[229]	DPen4	Oϵ2−N1[b] (3.5)	TM5−ligand

[a] Alternative cross-linking constraints between TM5 and -6 applied in models 1−5. The model number is given in parentheses. [b] From the C-terminal NH_2 group of the ligand.

results of spin-labeling studies (*22*) that evaluated distances between residues in TM3 (3.54) and TM6 (6.31−6.35) in the inactive and active states of rhodopsin (Table 7). To estimate the corresponding distances in all five models, the spin-labeled cysteines were incorporated at positions 169 (3.54), 276 (6.31), 277 (6.32), 278 (6.33), 279 (6.34), and

Table 7: Distances between Nitroxide Spin-Labels, Attached to Residues in Positions 169 (3.54) and 276−280 (6.31−6.35) in the Five Models of the μ-Opioid Receptor, Calculated with Different Cross-Linking Constraints between TM5 and TM6[a]

		estimated distance in the models of active states (Å)				
labeled residues of the μ-receptor	expected distance in the active state (Å)	model 1[b] (C256−C279)	model 2 (E258−C272−H276)	model 3 (C256−C280)	model 4 (C256−C281)	model 5 (C256−C282)
169−276	>16 (W)	14−16	14−18	16−18	13−19	15−19
169−277	10−16 (M)	11−16	11−16	15−19	6−12	10−16
169−278	4−9 (S)	7−12	5−9	8−15	4−10	5−8
169−279	>16 (W)	15−17	14−15	5−7	16−20	16−18
169−280	>16 (W)	15−18	16−19	15−19	13−18	16−19
rmsd (Å)[c]		1.81	1.98	2.28	2.60	2.49

[a] Distances that deviate from expected values, defined in the spin-labeling studies (*22*), are underlined. [b] The cross-linking constraints between TM5 and -6, included in calculations of each model, are given in parentheses. [c] The rmsd between inactive and active μ-receptor models (291 C_α atoms).

280 (6.35) of each model, and the ranges of •O−N···N−O• distances were measured in the sterically allowed conformers of the maleimide labels. The strengths of interactions between nitroxide radicals in the experiments were divided into three categories (*22*) that can be defined as "strong", "medium", and "weak" (S, M, and W, respectively). During activation of rhodopsin, the strengths of the interactions of nitroxides changed as follows for the five pairs of labeled residues indicated in Table 5 (169−276, 169−277, etc.) (*22*): S → W, M → M, M → S, S → W, and M → W. In the crystal structure of rhodopsin (PDB entry 1gzm), the strong interactions (3.54−6.31 and 3.54−6.34) correspond to distances of 4−10 and 5−7 Å, respectively, while the medium interactions (3.54−6.32, 3.54−6.33, and 3.54−6.35) are observed at 14−16, 13−16, and 9−13 Å, respectively. Thus, the S, M, and W interactions can be assigned to distances of 4−9, 10−16, and >16 Å, respectively. A comparison of the corresponding distances in the five different models of the active state indicates that only the fifth model, calculated with the 256−282 disulfide bridge, was completely consistent with the expected values. This model has a greatly shifted TM6, provides a large cavity on the cytoplasmic surface of the μ-receptor for binding with G proteins (*19*), and has the greatest accessibility to water of residues in TM5 (5.61, 5.64, and 5.65) that have been shown to be important for interactions with the G_α subunit (*27*). Therefore, model 5 was selected as the one most closely representing the active conformation.

During these calculations, we preserved the secondary structure of the inactive μ-receptor (similar to that in PDB entry 1gzm; see Figure 1). Thus, it was assumed that the intracellular parts of TM5 and -6 remain α-helical after activation. This assumption can be justified for the regions involved in disulfide cross-linking (models 1 and 3−5 in Table 7) by the results of spin-labeling experiments (*17*). For example, the mobilities of spin-labels attached to cysteine side chains in the region of residues 246−255 of rhodopsin (corresponding to residues 274−283 in TM6 of the μ-receptor) undergo very small changes, and their accessibilities follow an α-helical pattern in the active state of rhodopsin (*61*). However, α-helical regions that form a metal-binding site (model 2 in Table 7) could partially unfold during activation. Indeed, the last turns (258−265) of TM5 and the first turn (270−273) of TM6 (6.25−6.28) adopt either a coil or α-helical conformation in different crystal structures of rhodopsin (rhodopsin residues 229−236 and 242−245 of PDB entry 1f88 vs PDB entry 1gzm).

Figure 4 shows the superposition of the active and inactive state models. The active conformation has a strongly shifted TM6 (rmsd = 6.2 Å for 38 C^α atoms), slightly shifted TM1 and -3−5 (rmsd = 1.1−1.5 Å), and minor movements of TM2 and -7 (rmsd = 0.8 Å). TM6 moves away from TM3 and -7, and toward TM5; TM4 moves toward TM2, and helix 8 moves away from TM1. The changes occur primarily in the intracellular part of the transmembrane domain. The overall rmsd of the active and inactive conformations was relatively small [2.49 Å for all 291 C^α atoms of the μ-receptor (residues 64−354)]. The deviation from the TM domain of the rhodopsin structure (PDB entry 1gzm) was 2.2 Å for 212 common C^α atoms.

The movements of α-helices cause rotations of certain side chains, whose conformers were changed to avoid interatomic hindrances, to optimize packing, or to maximize the number of hydrogen bonds. Some of the rotating residues occupy the ligand binding pocket (Asp^{147}, Met^{151}, Glu^{229}, Lys^{233}, Trp^{293}, Tyr^{299}, Lys^{303}, and Trp^{318}), while others form helix−helix interfaces (Leu^{158}, Arg^{165}, Asn^{188}, Leu^{232}, Tyr^{252}, Met^{255}, Leu^{331}, Leu^{335}, Leu^{339}, Tyr^{326}, and Phe^{343}) or are situated in nonregular loops (Phe^{178} and Phe^{313}). Some of the rotating residues (Arg^{165}, Tyr^{252}, Trp^{293}, Tyr^{336}, and Phe^{343}) are highly conserved in the GPCR family and may be crucial for signal transduction. The most important of these is a conserved residue from the binding pocket, Trp^{293} (6.48). The indole ring may play the role of a conformational "trigger" when it changes its orientation ($\chi_2 \sim 0°$ instead of ~60°) and breaks an H-bond with Asn^{228} that is present in the inactive μ-receptor (*15*). The ionic interaction between Asp^{164} and Arg^{165} (TM3), which may stabilize the inactive state (*62*), is broken in the active state model. The rotation of Arg^{165} leads to formation of new H-bonds with the rotated Tyr^{252} (TM5), Tyr^{326} (TM7), and possibly the G protein G_α subunit in the active state. The H-bond between Thr^{279} (TM6) and Arg^{165} is also broken, allowing the shift of TM6 relative to TM3. This is consistent with the observed constitutive activity of the T279K mutant and the decreased level of activation of the T279D mutant of the μ-receptor (*63*). The disappearance of several H-bonds involving TM4 (Asn^{109}−Asn^{188*} and Tyr^{149}−Ser^{196*}) is associated with the tilting of TM4 in the active receptor. During the distance geometry calculations, side chains of three aromatic residues in TM3 (Tyr^{148}, Phe^{152}, and Phe^{156}) sometimes underwent a concerted rotation (their χ_1 angles simultaneously changed from −60° to 180°), which produced an even more pronounced tilt of TM4. The preliminary calculations indicate that such models are more

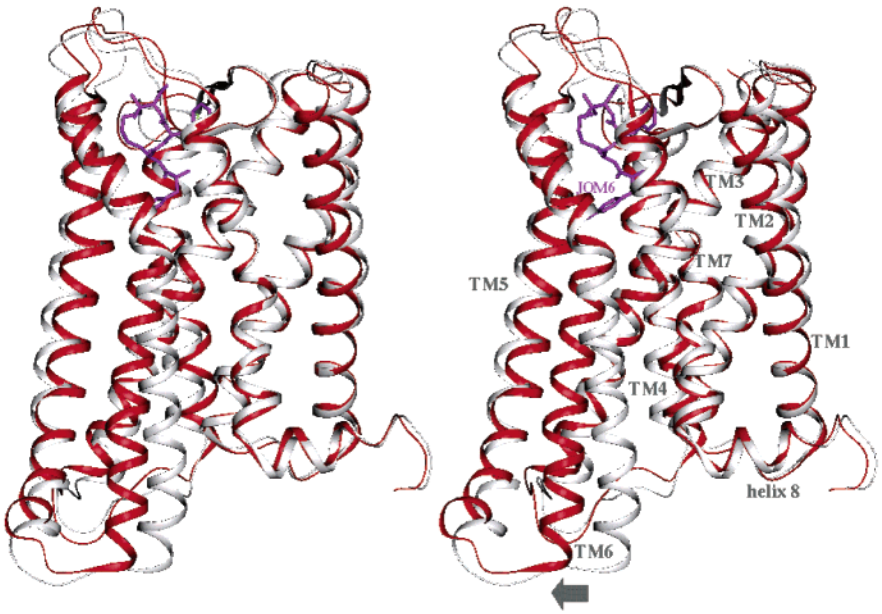

FIGURE 2: Stereoview of the superposition of TM helices of the inactive MOR model (white) with the active MOR−JOM6 model (red). JOM6 is colored magenta.

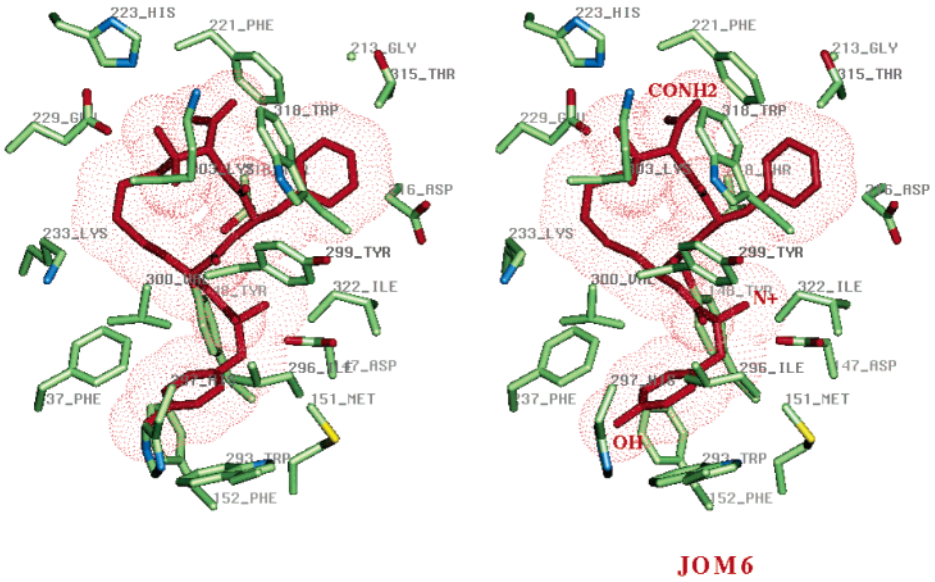

FIGURE 3: Stereoview of JOM6 (red) in the binding pocket of the active MOR (receptor residues are colored by element).

suitable for docking of morphine and oripavine alkaloid agonists.

Many side chain hydrogen bonds are rearranged as a result of the helix motions. Some are broken during activation (Asn^{104}−Tyr^{336*}, Asn^{109}−Asn^{188*}, Asp^{147*}−Thr^{120}, Asp^{147*}−Glu^{124}, Asp^{147*}−Tyr^{326*}, Tyr^{149}−Ser^{196*}, Asp^{150*}−Asn^{328}, Asp^{164*}−Arg^{165*}, Arg^{165*}−Thr^{279*}, Glu^{229}−Lys^{233*}, Arg^{277*}−Glu^{341*}, and Trp^{293*}−Asn^{328}), while others are newly formed in the active state model (Tyr^{106}−Asn^{183}, Asn^{150*}−Ser^{329}, Ser^{162}−Tyr^{252}, Arg^{165*}−Tyr^{252}, and Arg^{165*}−Tyr^{326*}). The asterisks denote residues whose replacement results in constitutive activation of opioid receptors (*54*, *64*−*66*). Most of these residues form H-bonds stabilizing the inactive conformation, which must be broken during the conformational transition.

The arrangement of JOM6 inside the binding pocket of the μ-receptor is presented in Figure 3. The peptide is in a bound conformation that was proposed previously and has the lowest-energy structure of the tripeptide cycle (see footnote 2) (*43*). The hydrophilic backbone of the peptide interacts with the polar area that is formed by Tyr^{148}, Thr^{218}, and Asp^{147} and may be saturated with a few bound water molecules. The N^+ group of Tyr^1 forms an ion pair with Asp^{147} (TM3) and participates in an amine−aromatic interaction with the proximal Tyr^{148}. The aromatic ring of Tyr^1 occupies a site formed by Tyr^{148}, Phe^{152}, Phe^{237}, Trp^{293}, His^{297}, Ile^{296}, and Val^{300} at the bottom of the binding cavity. The hydroxyl of Tyr^1 forms H-bonds with His^{297} (TM6) and with the backbone carbonyl of Ala^{240}, which is excluded from the system of intrahelical H-bonds in TM5 because of formation of an α-aneurism. The importance of Asp^{147}, His^{297}, Tyr^{148}, and Trp^{293} for binding of the peptide agonist has previously been demonstrated for opioid receptors (*67*−*74*). The C-terminal carboxamide of the ligand is in direct contact with the COO^- group of Glu^{229} (closest distance of ∼4 Å), and not far from the positively charged groups of

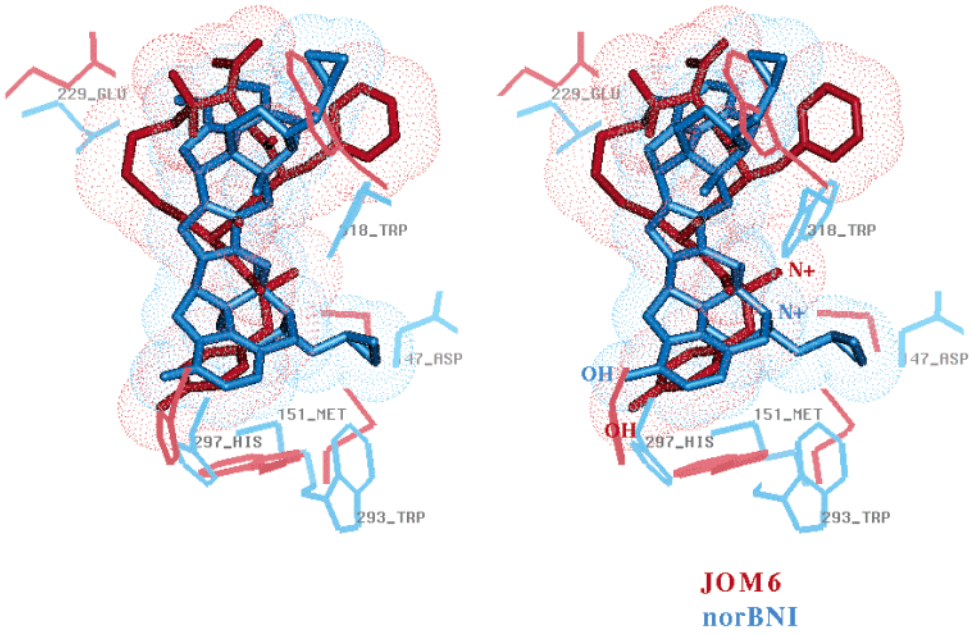

FIGURE 4: Stereoview of the superposition of inactive (blue) and active (red) state models of the μ-receptor with incorporated antagonist (norBNI, blue) and agonist (JOM6, red), respectively. Only ligands and a few important residues of the μ-receptor (Asp^{147}, Met^{151}, Glu^{229}, Trp^{293}, His^{297}, and Trp^{318}) are shown.

Lys^{303} and His^{223} (~5−7 and 4 Å, respectively). This explains the influence of the E229D mutation on binding of JOM6 and JOM18 (Table 4), the previously observed participation of Lys^{303} in the ligand binding pocket, and the adverse effect of His^{223} mutations or modification of free sulfhydryl groups by NEM on the binding of opiates (*75*).

The side chain of Phe^3 interacts with residues from extracellular loops EL2, EL3, and TM7: Gly^{213}, Asp^{216}, Phe^{221}, Thr^{315}, and Trp^{318}. The binding site of the Phe^3 residue is nonpolar and geometrically well-adapted for a planar aromatic group. Therefore, replacements with the charged imidazole or nonplanar aliphatic groups lead to peptides with lower binding affinities for the wild-type receptor (Table 2). However, the affinities are partially restored in the G213C/T315C double mutant (Table 2), most probably because of a direct stabilizing interaction between the C^{β}-S^{γ} group of Cys^{213} and side chains of His, Leu, and other residues substituting for Phe^3, as is apparent from inspection of the active state model. The Δ^EPhe^3 analogue of JOM6 has an only slightly lower affinity for the wild-type μ-receptor than does the parent peptide, while the affinity of Δ^ZPhe^3 is significantly reduced (Table 3), because the Phe aromatic ring is fixed in the proper $\chi_1 \sim 180°$ conformer in the *E*-configuration, versus the $\chi_1 \sim 0°$ in the *Z*-configuration, the latter resulting in adverse steric clashes.

The W318L mutant was designed for exploring μ- versus δ-selectivity, with respect to the role of Trp^{318} in selective binding of opioid ligands as had been suggested previously (*58*−*60*). Inspection of a model of this mutant suggests certain conformational rearrangements. The removal of the large Trp^{318} side chain creates a large hole in the protein core that can be filled by the spatially proximal aromatic side chain of Tyr^{299} from TM6 if it changes χ_1 from −60° to 180° (Tyr^{299} faces the lipid, when $\chi_1 = -60°$). The aromatic ring of the shifted Tyr^{299} favors a different (*gauche*+) conformer of the Leu^{318} side chain, which partially overlaps with Phe^3 of the ligand. The apparent interatomic hindrances can be relaxed in the parent peptide, but not in the more constrained Δ^ZPhe^3 analogue, which explains its poor binding to this mutant (Table 3). The reorientation of Trp^{318} and Tyr^{299} residues may influence the conformational changes in TM6 and -7 during activation. This agrees with the observed influence of Trp^{318} mutations not only on ligand binding but also on activation of opioid receptors (*59*).

Another residue that forms a contact with Phe^3 in the model is the charged Asp^{216}, which can form an intrinsic metal binding center with His^{319} (*15*). Substitution of Asp^{216} with a nonpolar Val residue improves affinities for the parent peptide and its Δ^EPhe^3 and Δ^ZPhe^3 analogues (Table 3), thus pointing to this interaction. The coordination of Zn^{2+} ions would require the side chain of Asp^{216} to change its χ_1 conformer and to occupy the area of space designed for the aromatic ring of Phe^3, which would interfere with binding of opioid ligands, as observed previously (*15*).

DISCUSSION

In this study, we have examined the complex of the μ-opioid receptor with its cyclic tetrapeptide agonist, Tyr^1-c(S-Et-S)[D-Cys^2-Phe^3-D-Pen^4]NH_2 (JOM6), using mutagenesis, engineered metal-binding centers, and computational modeling. The amino acid replacements were made simultaneously in the receptor and ligand to identify interacting pairs of residues, whose effects on binding are strongly nonadditive. All peptide analogues of JOM6 examined here have previously been shown to be μ-opioid receptor agonists (*37*−*41*, *43*) and thus are appropriate for probing the active state of the receptor.

Native and engineered Zn^{2+}-binding sites have been widely used to evaluate the relative proximity and the dynamics of transmembrane helices in GPCRs (*15*, *33*−*36*). These studies have exclusively employed receptor residues. The approach used in our study is novel in that both ligand and receptor residues simultaneously participate in Zn^{2+} binding. Two

zinc-binding centers were engineered between the receptor and peptide: His^{1}(JOM6)-V300C-H207 and His^{3}(JOM6)-G213C-T315C (as described in the Results). Furthermore, it was found that the Phe^{3} aromatic ring of the peptide interacts with Trp^{318} (TM7), while its C-terminal carboxamide group interacts with Glu^{229} (TM5). These structural constraints, together with the previously determined contact between the carboxyl of Asp^{147} (TM3) and the N^{+} group of the ligand (*67*, *71*, *73*), were applied for distance geometry modeling of the receptor−peptide complex. It is worth mentioning that, although many residues have been shown to affect the binding of opioid ligands (*3*, *4*, *76*, *77*), specific atomic contacts between opioid receptors and their ligands have previously been determined in only a few cases, such as cross-linking of the fumarate moiety of the irreversible μ-antagonist β-funaltraxamine to Lys^{233} (TM5) in the μ-receptor (*78*) and the interaction of the norbinaltorphimine (norBNI) N-17′ basic nitrogen atom with acidic Glu^{297} (TM6) in the κ-receptor or with the corresponding K303E of a μ-receptor mutant (*79*−*81*).

The binding of agonists triggers the activation of the μ-opioid receptor. The corresponding active state model with the bound peptide agonist was generated here by distance geometry using the structure of the inactive state of rhodopsin and a large number of experimental constraints from disulfide cross-linking and design of metal-binding centers. These constraints were combined from different rhodopsin-like GPCRs, assuming that they share a common conformation (*82*) and activation mechanism (*21*). This approach has been successfully applied for *ab initio* modeling of rhodopsin, when H-bond constraints between polar residues were combined from 410 GPCRs (*48*, *83*). The structural similarity of GPCR active states can also be expected, since a number of different GPCRs are activated by identical or similar ligands (*84*). The cross-linking constraints were supplemented by interhelical hydrogen bonds and protein−ligand contacts identified in this work.

The active state model of the μ-receptor can be compared with a homology model of the inactive state that was proposed previously (*15*). This comparison (Figure 4) suggests a specific activation pathway. The process begins with binding of the peptide agonist. The most important residue of the peptide is Tyr^{1}, whose N^{+} and hydroxyl groups form H-bonds with Asp^{147} (TM3) and His^{297}, respectively (the hydroxyl group also forms an H-bond with the backbone carbonyl of Ala^{240}). These interactions induce rotation of the Asp^{147} side chain. In the inactive state ($\chi_1 \sim -60°$), Asp^{147} forms H-bonds with Thr^{120}, Gln^{124}, and Tyr^{326}. In the active state ($\chi_1 \sim 180°$), Asp^{147} forms an ion pair (distance of <3.5 Å) with the agonist. Furthermore, agonist binding results in reorientations of several other side chains (Met^{151}, Glu^{229}, Lys^{233}, Trp^{293}, Tyr^{299}, Lys^{303}, and Trp^{318}) and small shifts of TM3−7 and EL2. The interactions of the antagonist (norBNI) with the inactive conformation are quite different. Its tyramine portion also forms an H-bond with His^{297}, but the N^{+} group is distant from the carboxyl of Asp^{147} (distance of ∼7 Å). The cyclopropylmethyl group of norBNI occupies the space between Trp^{293} and Tyr^{326}, which prevents the reorientation of Asp^{147} and formation of the corresponding ion pair. In the inactive state, His^{297} forms more extensive contacts with the ligand, while the ionic interaction between the N^{+} group of the ligand and Asp^{147} must be much weaker. This explains some important observations. For example, replacement of His^{297} with Asn had a larger impact on the binding of antagonists than agonists (*70*), while the D147A mutation had a significant adverse effect on the binding of agonists, but not antagonists (*71*). Furthermore, the presence of a protonated amine is especially important for agonists: their binding is optimal at neutral pH, while antagonists and partial agonists can also bind at alkaline pH, when their amine moiety is predominantly uncharged (*77*). The models also explain the recent observation of Schiller and colleagues that elimination of the N-terminal amino group converts a number of opioid peptide agonists to antagonists (*85*).

The rapid binding of agonist must be followed by slower rearrangement of transmembrane helices. The conserved Trp^{293} residue plays a key role here. During activation, it rotates to form an attractive "stacking" interaction with Tyr^{1} of JOM6 (χ_2 of Trp^{293} changes from ∼60° to ∼0°). In the inactive state model, the position of Trp^{293} is locked by interaction with the cyclopropylmethyl group of norBNI (Figure 4). The rearrangement of Trp^{293} must be accompanied by an ∼20° counterclockwise rotation (as viewed from the extracellular side) of TM6 to avoid a collision of Trp^{293} with TM3. This opens up a polar crevice among TM3, -6, and -7 that can be partially filled by water. The rigid-body rotation of TM6 and formation of the water-filled cavity weaken the packing of TM6 with TM3 and -7. Therefore, TM6 moves to an alternative spatial position and associates with TM5, where the conserved Phe^{289} (6.44) is positioned between TM3 and -5 instead of between TM3 and -7, as in the inactive state. The helix movement is accompanied by the rotation of polar conserved residues on the cytoplasmic side of the α-bundle (Arg^{165}, Tyr^{252}, and Tyr^{326}) and the rearrangement of the H-bond network between TM3 and TM5−7. The rigid-body movement of TM6 induces smaller shifts of all the other helices near the cytoplasmic surface and opens a large cavity that can be occupied by the C-terminal α-helix of the G protein (*27*) (Figure 5).

Thus, GPCR activation would include at least two separate steps: (1) the rapid binding of ligand, which is accompanied by reorientation of several side chains in the binding pocket (such as Asp^{147}, Met^{151}, Glu^{229}, Lys^{233}, Tyr^{299}, Lys^{303}, and Trp^{318}) and small movements of surrounding helices, and (2) a large-scale, slower motion of TM6 that is simultaneous with rotation of Trp^{293} and several other side chains (Leu^{158}, Arg^{165}, Tyr^{252}, Tyr^{326}, and Phe^{343}), closer to the intracellular surface, which is accompanied by rearrangement of a hydrogen bonding network (see the Results). Such a mechanism is supported by recent studies of multistep activation in the β_2-adrenergic receptor (*7*). Surprisingly, four alternative disulfide bonds can be formed between TM5 and -6 in the presence of the agonist (Table 5 and ref *32*). This suggests some flexibility of TM6 in the active receptor. The existence of multiple ligand-specific active states of the receptor with distinct cellular functions has been proposed recently on the basis of the results of fluorescent studies of the β_2-adrenoreceptor (*5*−*7*) and differential effects of cross-linking on the activation of G proteins and kinases (*26*).

This proposed activation mechanism and the model of the active μ-receptor are in agreement with extant experimental data that were not applied during our distance geometry calculations. First, a significant movement of the conserved Trp (6.48) residue has been detected in rhodopsin and

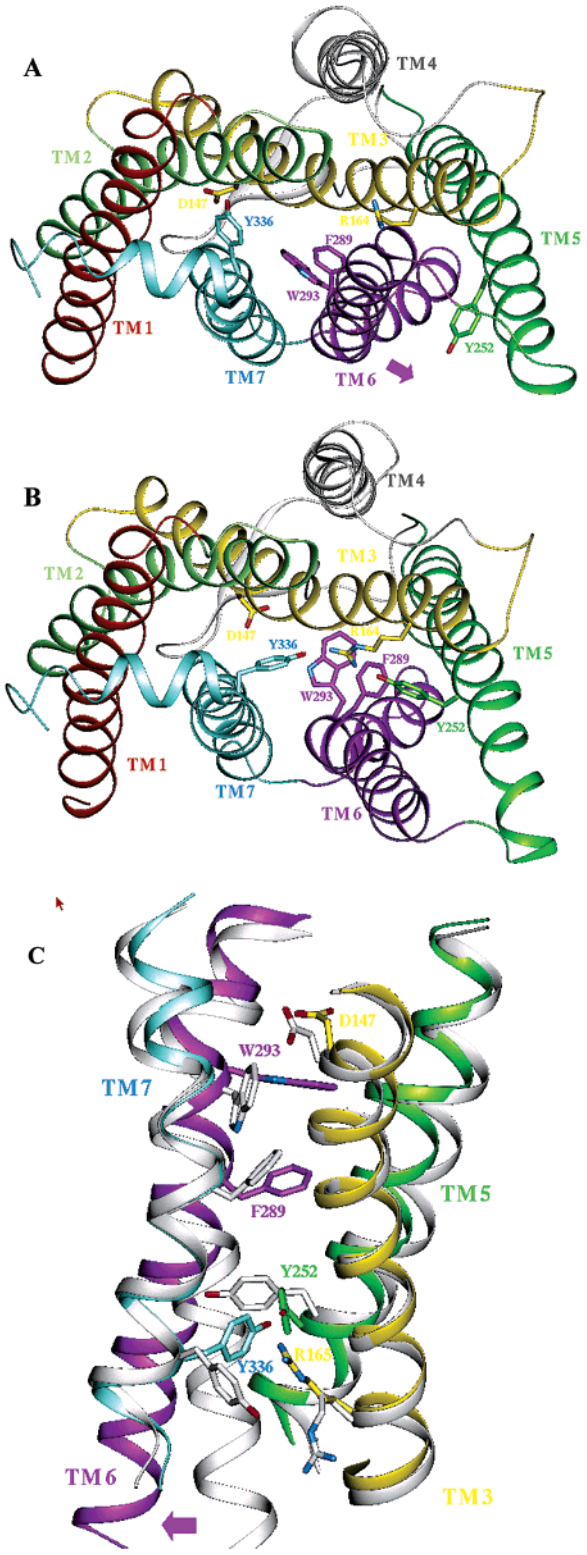

FIGURE 5: Top view (from the cytoplasm) of the μ-opioid receptor models in the inactive (A) and active (B) conformations. Transmembrane helices are shown in ribbon representations. The functionally important residues, whose spatial positions change upon receptor activation (Asp^{147}, Arg^{165}, Tyr^{252}, Phe^{289}, Trp^{293}, and Tyr^{336}), are shown in licorice representations. (C) Side view of the fragments of four helices (TM3 and -5−7) of the μ-opioid receptor models in the inactive (white) and active (helices colored yellow, green, magenta, and cyan, respectively) conformations. The functionally important residues, whose spatial position changes upon receptor activations (Asp^{147}, Arg^{165}, Tyr^{252}, Phe^{289}, Trp^{293}, and Tyr^{336}), are shown in licorice representations.

leukotriene receptors (*28*, *86*, *87*, *93*). Second, the estimation of interhelical distances using cross-linking, spin-labeling, and fluorescence studies indicates that the intracellular end of TM6 moves away from TM3 and TM7 and closer to TM5 (*5*, *22*, *24*−*26*, *32*), while TM4 moves slightly closer to TM2 (*17*), exactly as in our model. For example, the experimental distances between spin-labels attached to positions 3.54 and 6.31−6.35 correlate with the corresponding distances in our model (Table 5). Moreover, the increase in the $C^{\beta}\cdots C^{\beta}$ distances between residues 169 in TM3 (3.54) and 276 in TM6 (6.31) from 7 to 14 Å or between residues 274 in TM6 (6.29) and 342 in TM7 (7.59) from 9 to 15 Å in the active μ-receptor model is in good agreement with the observation that the corresponding disulfide cross-linking impairs signal transduction (*26*). Third, our model of the active state explains the experimentally observed changes in residue mobility and accessibility: (a) decreased mobility of residues in TM5 (positions 5.62 and 5.66) and increased mobility of residues in TM6 (positions 6.33, 6.34, and 6.36) (*61*), (b) increased accessibility of residues at the inner face of TM5 (position 5.64) and TM6 (positions 6.36, 6.37, 6.40, 6.41, and 6.44) to chemical modification (*61*, *87*), (c) shift of residues at positions 6.33 and 6.34 from the vicinity of Arg (3.50) to the more nonpolar environment at the helix 5−helix 6 interface (*24*, *88*), (d) burial of Cys (6.27) in a hydrophobic environment and its approach toward TM5 (*5*), and (e) accessibility of the TM5 inner face (positions 5.61, 5.64, and 5.65) for interaction with the C-terminal peptide of the G_{α} subunit (*27*). Fourth, the decrease in the number of interhelical H-bonds (see the Results) and the opening of the α-bundle from the intracellular side could result in increased flexibility and decreased stability of the active state, which is in agreement with many observations (*6*, *89*, *90*). Interestingly, interhelical H-bonds, broken in the active state model, are formed by residues whose replacements are known to produce constitutively active mutants (*54*, *64*−*66*, *76*). Consequently, increased structural instability could be expected for constitutively active mutants that involve H-bonded polar residues, which indeed has been experimentally demonstrated (*89*). Fifth, the proposed model of the μ-receptor with JOM6 satisfies all specific receptor−ligand interactions identified in this work and explains numerous mutagenesis results (see above) and data on the distinct effect of mutation on agonist or antagonist binding (*70*, *71*, *77*). Finally, the receptor-bound conformation of the cyclic peptide, which has been proposed previously solely on the basis of conformation−activity relationships of the ligand (*43*), is complementary to the receptor model.

It must be emphasized that our model of the μ-opioid receptor was constructed by distance geometry calculations with various constraints, rather than by theoretical methods. It appears to be completely different from the published theoretical models of the active state of rhodopsin and metarhodopsin II (*91*, *92*) with available atomic coordinates (PDB entries 1ln6 and 1ov1, respectively). In these models, almost all helices are largely shifted, resulting in rmsds from the inactive rhodopsin transmembrane helices (PDB entry 1gzm) of 5.7 and 4.3 Å, respectively, i.e., much larger than the rmsd of 2.2 Å for our model. These theoretical models are inconsistent with experimental data discussed above that pointed to significant motion of only TM6 (*17*). Moreover, the rigid-body shift and rotation of TM5 in PDB entry 1ov1

substantially changes the geometry of the binding pocket and brings the residues that are important for agonist binding in other GPCRs (*7*) into the lipid.

In conclusion, this study represents the first detailed structural analysis of the interactions of a peptide agonist with the μ-opioid receptor. The experimental constraints that were obtained, together with published cross-linking data, allowed modeling of the active state in a complex with the μ-selective peptide agonist, by distance geometry. The resulting realistic model of the μ-receptor [available from our web site (http://mosberglab.phar.umich.edu/resources/index.php)] can be applied as a structural template for experimental and modeling studies of μ-, δ-, and κ-opioid and orphanine opioid receptors with different peptide or alkaloid agonists, and eventually for rational drug design. Moreover, the proposed model can also serve as a structural template of the active state of other rhodopsin-like GPCRs, while the crystal structures of rhodopsin provide the template for inactive receptors.

ACKNOWLEDGMENT

We are grateful to Huda Akil for making the μ-receptor expression vector available to us.

REFERENCES

1. Kieffer, B. L. (2000) Opioid receptors: from genes to mice, *J. Pain 1* (Suppl. 3), 45−50.
2. Burford, N. T., Tolbert, L. M., and Sadee, W. (1998) Specific G protein activation and μ-opioid receptor internalization caused by morphine, DAMGO and endomorphin I, *Eur. J. Pharmacol. 342*, 123−126.
3. Quock, R. M., Burkey, T. H., Varga, E., Hosohata, Y., Hosohata, K., Cowell, S. M., Slate, C. A., Ehlert, F. J., Roeske, W. R., and Yamamura, H. I. (1999) The δ-opioid receptor: molecular pharmacology, signal transduction, and the determination of drug efficacy, *Pharmacol. Rev. 51*, 503−532.
4. Waldhoer, M., Bartlett, S. E., and Whistler, J. L. (2004) Opioid receptors, *Annu. Rev. Biochem. 73*, 953−990.
5. Ghanouni, P., Steenhuis, J. J., Farrens, D. L., and Kobilka, B. K. (2001) Agonist-induced conformational changes in the G-protein-coupling domain of the β2 adrenergic receptor, *Proc. Natl. Acad. Sci. U.S.A. 98*, 5997−6002.
6. Ghanouni, P., Gryczynski, Z., Steenhuis, J. J., Lee, T. W., Farrens, D. L., Lakowicz, J. R., and Kobilka, B. K. (2001) Functionally different agonists induce distinct conformations in the G protein coupling domain of the β2 adrenergic receptor, *J. Biol. Chem. 276*, 24433−24436.
7. Swaminath, G., Xiang, Y., Lee, T. W., Steenhuis, J., Parnot, C., and Kobilka, B. K. (2004) Sequential binding of agonists to the β2 adrenoceptor. Kinetic evidence for intermediate conformational states, *J. Biol. Chem. 279*, 686−691.
8. Ballesteros, J. A., and Weinstein, H. (1995) Integrated methods for the construction of three-dimensional models and computational probing of structure−function relations in G-protein coupled receptors, *Methods Neurosci. 25*, 366−428.
9. Gershengorn, M. C., and Osman, R. (2001) Minireview: Insights into G protein-coupled receptor function using molecular models, *Endocrinology 142*, 2−10.
10. Stenkamp, R. E., Filipek, S., Driessen, C. A., Teller, D. C., and Palczewski, K. (2002) Crystal structure of rhodopsin: a template for cone visual pigments and other G protein-coupled receptors, *Biochim. Biophys. Acta 1565*, 168−182.
11. Filipek, S., Teller, D. C., Palczewski, K., and Stenkamp, R. (2003) The crystallographic model of rhodopsin and its use in studies of other G protein-coupled receptors, *Annu. Rev. Biophys. Biomol. Struct. 32*, 375−397.
12. Berman, H. M., Westbrook, J., Feng, Z., Gilliland, G., Bhat, T. N., Weissig, H., Shindyalov, I. N., and Bourne, P. E. (2000) The Protein Data Bank, *Nucleic Acids Res. 28*, 235−242.
13. Riek, R. P., Rigoutsos, I., Novotny, J., and Graham, R. M. (2001) Non-α-helical elements modulate polytopic membrane protein architecture, *J. Mol. Biol. 306*, 349−362.
14. Archer, E., Maigret, B., Escrieut, C., Pradayrol, L., and Fourmy, D. (2003) Rhodopsin crystal: new template yielding realistic models of G-protein-coupled receptors? *Trends Pharmacol. Sci. 24*, 36−40.
15. Fowler, C. B., Pogozheva, I. D., LeVine, H., III, and Mosberg, H. I. (2004) Refinement of a Homology Model of the μ-Opioid Receptor Using Distance Constraints from Intrinsic and Engineered Zinc-Binding Sites, *Biochemistry 43*, 8700−8710.
16. Okada, T., Ernst, O. P., Palczewski, K., and Hofmann, K. P. (2001) Activation of rhodopsin: new insights from structural and biochemical studies, *Trends Biochem. Sci. 26*, 318−324.
17. Hubbell, W. L., Altenbach, C., Hubbell, C. M., and Khorana, H. G. (2003) Rhodopsin structure, dynamics, and activation: a perspective from crystallography, site-directed spin labeling, sulfhydryl reactivity, and disulfide cross-linking, *Adv. Protein Chem. 63*, 243−290.
18. Gether, U. (2000) Uncovering molecular mechanisms involved in activation of G protein-coupled receptors, *Endocr. Rev. 21*, 90−113.
19. Meng, E. C., and Bourne, H. R. (2001) Receptor activation: what does the rhodopsin structure tell us? *Trends Pharmacol. Sci. 22*, 587−593.
20. Parnot, C., Miserey-Lenkei, S., Bardin, S., Corvol, P., and Clauser, E. (2002) Lessons from constitutively active mutants of G protein-coupled receptors, *Trends Endocrinol. Metab. 13*, 336−343.
21. Karnik, S. S., Gogonea, C., Patil, S., Saad, Y., and Takezako, T. (2003) Activation of G-protein-coupled receptors: a common molecular mechanism, *Trends Endocrinol. Metab. 14*, 431−437.
22. Farrens, D. L., Altenbach, C., Yang, K., Hubbell, W. L., and Khorana, H. G. (1996) Conformational changes in rhodopsin. Movement of helix f detected by site-specific chemical labeling and fluorescence spectroscopy, *J. Biol. Chem. 274*, 1683−1690.
23. Gether, U., Lin, S., Ghanouni, P., Ballesteros, J. A., Weinstein, H., and Kobilka, B. K. (1997) Agonists induce conformational changes in transmembrane domains III and VI of the β2 adrenoceptor, *EMBO J. 16*, 6737−6747.
24. Dunham, T. D., and Farrens, D. L. (1999) Conformational changes in rhodopsin. Movement of helix f detected by site-specific chemical labeling and fluorescence spectroscopy, *J. Biol. Chem. 274*, 1683−1690.
25. Han, M., Smith, S. O., and Sakmar, T. P. (1998) Constitutive activation of opsin by mutation of methionine 257 on transmembrane helix 6, *Biochemistry 37*, 8253−8261.
26. Cai, K., Klein-Seetharaman, J., Hwa, J., Hubbell, W. L., and Khorana, H. G. (1999) Structure and function in rhodopsin: effects of disulfide cross-links in the cytoplasmic face of rhodopsin on transducin activation and phosphorylation by rhodopsin kinase, *Biochemistry 38*, 12893−12898.
27. Janz, J. M., and Farrens, D. L. (2004) Rhodopsin activation exposes a key hydrophobic binding site for the transducin α-subunit C-terminus, *J. Biol. Chem. 279*, 29767−29773.
28. Lin, S. W., and Sakmar, T. P. (1996) Specific tryptophan UV-absorbance changes are probes of the transition of rhodopsin to its active state, *Biochemistry 35*, 11149−11159.
29. Altenbach, C., Klein-Seetharaman, J., Hwa, J., Khorana, H. G., and Hubbell, W. L. (1999) Structural features and light-dependent changes in the sequence 59−75 connecting helices I and II in rhodopsin: a site-directed spin-labeling study, *Biochemistry 38*, 7945−7949.
30. Altenbach, C., Cai, K., Klein-Seetharaman, J., Khorana, H. G., and Hubbell, W. L. (2001) Structure and function in rhodopsin: mapping light-dependent changes in distance between residue 65 in helix TM1 and residues in the sequence 306−319 at the cytoplasmic end of helix TM7 and in helix H8, *Biochemistry 40*, 15483−15492.
31. Altenbach, C., Klein-Seetharaman, J., Cai, K., Khorana, H. G., and Hubbell, W. L. (2001) Structure and function in rhodopsin: mapping light-dependent changes in distance between residue 316 in helix 8 and residues in the sequence 60−75, covering the cytoplasmic end of helices TM1 and TM2 and their connection loop CL1, *Biochemistry 40*, 15493−15500.
32. Ward, S. D., Hamdan, F. F., Bloodworth, L. M., and Wess, J. (2002) Conformational changes that occur during M3 muscarinic acetylcholine receptor activation probed by the use of an in situ disulfide cross-linking strategy, *J. Biol. Chem. 277*, 2247−2257.

33. Swaminath, G., Lee, T. W., and Kobilka, B. (2003) Identification of an allosteric binding site for Zn^{2+} on the β2 adrenergic receptor, *J. Biol. Chem. 278*, 352−356.
34. Elling, C. E., Thirstrup, K., Holst, B., and Schwartz, T. W. (1999) Conversion of agonist site to metal-ion chelator site in the β2-adrenergic receptor, *Proc. Natl. Acad. Sci. U.S.A. 96*, 12322−12327.
35. Holst, B., Elling, C. E., and Schwartz, T. W. (2000) Partial agonism through a zinc-ion switch constructed between transmembrane domains III and VII in the tachykinin NK(1) receptor, *Mol. Pharmacol. 58*, 263−270.
36. Lagerstrom, M. C., Klovins, J., Fredriksson, R., Fridmanis, D., Haitina, T., Ling, M. K., Berglund, M. M., and Schioth, H. B. (2003) High affinity agonistic metal ion binding sites within the melanocortin 4 receptor illustrate conformational change of transmembrane region 3, *J. Biol. Chem. 278*, 51521−51526.
37. Mosberg, H. I., Omnaas, J. R., Medzihradsky, F., and Smith, C. B. (1988) Cyclic, disulfide- and dithioether-containing opioid tetrapeptides: development of a ligand with high δ opioid receptor selectivity and affinity, *Life Sci. 43*, 1013−1020.
38. McFadyen, I. J., Sobczyk-Kojiro, K., Schaefer, M. J., Ho, J. C., Omnaas, J. R., Mosberg, H. I., and Traynor, J. R. (2000) Tetrapeptide derivatives of [D-Pen(2),D-Pen(5)]-enkephalin (DPDPE) lacking an N-terminal tyrosine residue are agonists at the μ-opioid receptor, *J. Pharmacol. Exp. Ther. 295*, 960−966.
39. Mosberg, H. I., Lomize, A. L., Wang, C., Kroona, H., Heyl, D. L., Ma, W., Sobczyk-Kojiro, K., Mousigian, C., and Porreca, F. (1994) Development of a model for the δ-opioid receptor pharmacophore. 1. Conformationally restricted Tyr^1 replacements in the cyclic δ receptor selective tetrapeptide Tyr-c[D-Cys-Phe-D-Pen]OH (JOM-13), *J. Med. Chem. 37*, 4371−4383.
40. Mosberg, H. I., Omnaas, J. R., Lomize, A., Heyl, D. L., Nordan, I., Mousigian, C., Davis, P., and Porreca, F. (1994) Development of a model for the δ opioid receptor pharmacophore. 2. Conformationally restricted Phe^3 replacements in the cyclic δ-receptor selective tetrapeptide Tyr-c[D-Cys-Phe-D-Pen]OH (JOM-13), *J. Med. Chem. 37*, 4384−4391.
41. Mosberg, H. I., Dua, R. K., Pogozheva, I. D., and Lomize, A. L. (1996) Development of a model for the δ opioid receptor pharmacophore: 4. Residue 3 dehydrophenyl-alanine analogs of Tyr-c[D-Cys-Phe-D-Pen]OH (JOM-13) confirm required *gauche* orientation of aromatic side chain, *Biopolymers 39*, 287−296.
42. Lomize, A. L., Flippen-Anderson, J. L., George, C., and Mosberg, H. I. (1994) Conformational analysis of the δ receptor-selective, cyclic opioid peptide,Tyr-c[D-Cys-Phe-D-Pen]OH(JOM-13). Comparison of X-ray crystallographic structures, molecular mechanics simulations and ^{1}H NMR data, *J. Am. Chem. Soc. 116*, 429−436.
43. Ho, J. C. (1997) Development of a model for the δ-opioid receptor pharmacophore, Ph.D. Thesis, University of Michigan, Ann Arbor, MI.
44. Mansour, A., Hoversten, M. T., Taylor, L. P., Watson, S. J., and Akil, H. (1995) The cloned μ, δ and κ receptors and their endogenous ligands: evidence for two opioid peptide recognition cores, *Brain Res. 700*, 89−98.
45. Bradford, M. M. (1976) A rapid and sensitive method for the quantitation of microgram quantities of protein utilizing the principle of protein-dye binding, *Anal. Biochem. 72*, 248−254.
46. Cheng, Y., and Prusoff, W. H. (1973) Relationship between inhibition constant (K_I) and concentration of inhibitor which causes 50% inhibition (I_{50}) of an enzymatic reaction, *Biochem. Pharmacol. 22*, 3099−3108.
47. Güntert, P., and Wüthrich, K. (1991) Improved efficiency of protein structure calculations from NMR data using the program DIANA with redundant dihedral angle constraints, *J. Biomol. NMR 1*, 447−456.
48. Pogozheva, I. D., Lomize, A. L., and Mosberg, H. I. (1997) The transmembrane 7 α-bundle of rhodopsin: distance geometry calculations with hydrogen bonding constraints, *Biophys. J. 72*, 1963−1985.
49. Pogozheva, I. D., Lomize, A. L., and Mosberg, H. I. (1998) Opioid receptor three-dimensional structures from distance geometry calculations with hydrogen bonding constraints, *Biophys. J. 75*, 612−634.
50. Munshi, U. M., Pogozheva, I. D., and Menon, K. M. (2003) Highly conserved serine in the third transmembrane helix of the luteinizing hormone/human chorionic gonadotropin receptor regulates receptor activation, *Biochemistry 42*, 3708−3715.
51. Zhang, P., Johnson, P. S., Zollner, C., Wang, W., Wang, Z., Montes, A. E., Seidleck, B. K., Blaschak, C. J., and Surratt, C. K. (1999) Mutation of human μ opioid receptor extracellular "disulfide cysteine" residues alters ligand binding but does not prevent receptor targeting to the cell plasma membrane, *Brain Res. Mol. Brain Res. 72*, 195−204.
52. Yu, H., and Oprian, D. D. (1999) Tertiary interactions between transmembrane segments 3 and 5 near the cytoplasmic side of rhodopsin, *Biochemistry 38*, 12033−12040.
53. Struthers, M., Yu, H., and Oprian, D. D. (2000) G protein-coupled receptor activation: analysis of a highly constrained, "straitjacketed" rhodopsin, *Biochemistry 39*, 7938−7942.
54. DeCaillot, F. M., Befort, K., Filliol, D., Yue, S., Walker, P., and Kieffer, B. L. (2003) Opioid receptor random mutagenesis reveals a mechanism for G protein-coupled receptor activation, *Nat. Struct. Biol. 10*, 629−636.
55. Brooks, B. R., Bruccoleri, E. R., Olafson, E. R., States, D. J., Swaminathan, S., and Karplus, M. (1983) CHARMM: A program for macromolecular energy, minimization and dynamics calculations, *J. Comput. Chem. 4*, 187−217.
56. Momany, F. A., and Rone, R. (1992) Validation of the general purpose QUANTA3.2/CHARMm force field, *J. Comput. Chem. 13*, 888−900.
57. Mosberg, H. I., and Fowler, C. B. (2002) Development and validation of opioid ligand−receptor interaction models: the structural basis of μ vs δ selectivity, *J. Pept. Res. 60*, 329−335.
58. Xu, H., Lu, Y. F., Partilla, J. S., Zheng, Q. X., Wang, J. B., Brine, G. A., Carroll, F. I., Rice, K. C., Chen, K. X., Chi, Z. Q., and Rothman, R. B. (1999) Opioid peptide receptor studies, 11: involvement of Tyr148, Trp318 and His319 of the rat μ-opioid receptor in binding of μ-selective ligands, *Synapse 32*, 23−28.
59. Bonner, G., Meng, F., and Akil, H. (2000) Selectivity of μ-opioid receptor determined by interfacial residues near third extracellular loop, *Eur. J. Pharmacol. 403*, 37−44.
60. Ulens, C., Van Boven, M., Daenens, P., and Tytgat, J. (2000) Interaction of *p*-fluorofentanyl on cloned human opioid receptors and exploration of the role of Trp-318 and His-319 in μ-opioid receptor selectivity, *J. Pharmacol. Exp. Ther. 294*, 1024−1033.
61. Altenbach, C., Yang, K., Farrens, D. L., Farahbakhsh, Z. T., Khorana, H. G., and Hubbell, W. L. (1996) Structural features and light-dependent changes in the cytoplasmic interhelical E−F loop region of rhodopsin: A site-directed spin-labeling study, *Biochemistry 35*, 12470−12478.
62. Li, J., Huang, P., Chen, C., de Riel, J. K., Weinstein, H., and Liu-Chen, L. Y. (2001) Constitutive activation of the μ opioid receptor by mutation of D3.49(164), but not D3.32(147): D3.49(164) is critical for stabilization of the inactive form of the receptor and for its expression, *Biochemistry 40*, 12039−12050.
63. Huang, P., Li, J., Chen, C., Visiers, I., Weinstein, H., and Liu-Chen, L. Y. (2001) Functional role of a conserved motif in TM6 of the rat μ opioid receptor: constitutively active and inactive receptors result from substitutions of Thr6.34(279) with Lys and Asp, *Biochemistry 40*, 13501−13509.
64. Claude, P. A., Wotta, D. R., Zhang, X. H., Prather, P. L., McGinn, T. M., Erickson, L. J., Loh, H. H., and Law, P. Y. (1996) Mutation of a conserved serine in TM4 of opioid receptors confers full agonistic properties to classical antagonists, *Proc. Natl. Acad. Sci. U.S.A. 93*, 5715−5719.
65. Befort, K., Zilliox, C., Filliol, D., Yue, S., and Kieffer, B. L. (1999) Constitutive activation of the δ opioid receptor by mutations in transmembrane domains III and VII, *J. Biol. Chem. 274*, 18574−18581.
66. Kam, K. W., New, D. C., and Wong, Y. H. (2002) Constitutive activation of the opioid receptor-like (ORL1) receptor by mutation of Asn133 to tryptophan in the third transmembrane region, *J. Neurochem. 83*, 1461−1470.
67. Surratt, C. K., Johnson, P. S., Moriwaki, A., Seidleck, B. K., Blaschak, C. J., Wang, J. B., and Uhl, G. R. (1994) μ opiate receptor. Charged transmembrane domain amino acids are critical for agonist recognition and intrinsic activity, *J. Biol. Chem. 269*, 20548−20553.
68. Mansour, A., Taylor, L. P., Fine, J. L., Thompson, R. C., Hoversten, M. T., Mosberg, H. I., Watson, S. J., and Akil, H. (1997) Key residues defining the μ-opioid receptor binding pocket: a site-directed mutagenesis study, *J. Neurochem. 68*, 344−353.
69. Spivak, C. E., Beglan, C. L., Seidleck, B. K., Hirshbein, L. D., Blaschak, C. J., Uhl, G. R., and Surratt, C. K. (1997) Naloxone

activation of μ-opioid receptors mutated at a histidine residue lining the opioid binding cavity, *Mol. Pharmacol. 52*, 983−992.
70. Bot, G., Blake, A. D., Li, S., and Reisine, T. (1998) Mutagenesis of a single amino acid in the rat μ-opioid receptor discriminates ligand binding, *J. Neurochem. 70*, 358−365.
71. Befort, K., Tabbara, L., Bausch, S., Chavkin, C., Evans, C., and Kieffer, B. (1996) The conserved aspartate residue in the third putative transmembrane domain of the δ-opioid receptor is not the anionic counterpart for cationic opiate binding but is a constituent of the receptor binding site, *Mol. Pharmacol. 49*, 216−223.
72. Befort, K., Tabbara, L., Kling, D., Maigret, B., and Kieffer, B. L. (1996) Role of aromatic transmembrane residues of the δ-opioid receptor in ligand recognition, *J. Biol. Chem. 271*, 10161−10168.
73. Li, J. G., Chen, C., Yin, J., Rice, K., Zhang, Y., Matecka, D., de Riel, J. K., DesJarlais, R. L., and Liu-Chen, L. Y. (1999) Asp147 in the third transmembrane helix of the rat μ opioid receptor forms ion-pairing with morphine and naltrexone, *Life Sci. 65*, 175−185.
74. Mouledous, L., Topham, C. M., Moisand, C., Mollereau, C., and Meunier, J. C. (2000) Functional inactivation of the nociceptin receptor by alanine substitution of glutamine 286 at the C terminus of transmembrane segment VI: evidence from a site-directed mutagenesis study of the ORL1 receptor transmembrane-binding domain, *Mol. Pharmacol. 57*, 495−502.
75. Shahrestanifar, M., Wang, W. W., and Howells, R. D. (1996) Studies on inhibition of μ and δ opioid receptor binding by dithiothreitol and *N*-ethylmaleimide. His223 is critical for mu opioid receptor binding and inactivation by *N*-ethylmaleimide, *J. Biol. Chem. 271*, 5505−5512.
76. Law, P. Y., Wong, Y. H., and Loh, H. H. (1999) Mutational analysis of the structure and function of opioid receptors, *Biopolymers 51*, 440−455.
77. Chaturvedi, K., Christoffers, K. H., Singh, K., and Howells, R. D. (2000) Structure and regulation of opioid receptors, *Biopolymers 55*, 334−346.
78. Chen, C., Yin, J., Riel, J. K., DesJarlais, R. L., Raveglia, L. F., Zhu, J., and Liu-Chen, L. Y. (1996) Determination of the amino acid residue involved in [^{3}H]β-funaltrexamine covalent binding in the cloned rat μ-opioid receptor, *J. Biol. Chem. 271*, 21422−21429.
79. Hjorth, S. A., Thirstrup, K., Grandy, D. K., and Schwartz, T. W. (1995) Analysis of selective binding epitopes for the κ-opioid receptor antagonist nor-binaltorphimine, *Mol. Pharmacol. 47*, 1089−1094.
80. Jones, R. M., Hjorth, S. A., Schwartz, T. W., and Portoghese, P. S. (1998) Mutational evidence for a common κ antagonist binding pocket in the wild-type κ and mutant μ[K303E] opioid receptors, *J. Med. Chem. 41*, 4911−4914.
81. Larson, D. L., Jones, R. M., Hjorth, S. A., Schwartz, T. W., and Portoghese, P. S. (2000) Binding of norbinaltorphimine (norBNI) congeners to wild-type and mutant μ and κ opioid receptors: molecular recognition loci for the pharmacophore and address components of κ antagonists, *J. Med. Chem. 43*, 1573−1576.
82. Ballesteros, J. A., Shi, L., and Javitch, J. A. (2001) Structural mimicry in G protein-coupled receptors: implications of the high-resolution structure of rhodopsin for structure−function analysis of rhodopsin-like receptors, *Mol. Pharmacol. 60*, 1−19.
83. Lomize, A. L., Pogozheva, I. D., and Mosberg, H. I. (1999) Structural organization of G-protein-coupled receptors, *J. Comput.-Aided Mol. Des. 13*, 325−353.
84. Bondensgaard, K., Ankersen, M., Thogersen, H., Hansen, B. S., Wulff, B. S., and Bywater, R. P. (2004) Recognition of privileged structures by G-protein coupled receptors, *J. Med. Chem. 47*, 888−899.
85. Schiller, P. W., Weltrowska, G., Nguyen, T. M.-D., Lemieux, C., Chung, N. N., and Lu, Y. (2003) Conversion of δ-, κ- and μ-receptor selective opioid peptide agonists into δ-, κ- and μ-receptor selective antagonists, *Life Sci. 73*, 691−698.
86. Chabre, M., and Breton, J. (1979) Orientation of aromatic residues in rhodopsin. Rotation of one tryptophan upon the meta I to meta II transition afer illumination, *Photochem. Photobiol. 30*, 295−299.
87. Baneres, J. L., Martin, A., Hullot, P., Girard, J. P., Rossi, J. C., and Parello, J. (2003) Structure-based analysis of GPCR function: conformational adaptation of both agonist and receptor upon leukotriene B4 binding to recombinant BLT1, *J. Mol. Biol. 329*, 801−814.
88. Gether, U., Asmar, F., Meinild, A. K., and Rasmussen, S. G. (2002) Structural basis for activation of G-protein-coupled receptors, *Pharmacol. Toxicol. 91*, 304−312.
89. Gether, U., Ballesteros, J. A., Seifert, R., Sanders-Bush, E., Weinstein, H., and Kobilka, B. K. (1997) Structural instability of a constitutively active G protein-coupled receptor. Agonist-independent activation due to conformational flexibility, *J. Biol. Chem. 272*, 2587−2590.
90. Abdulaev, N. G., and Ridge, K. D. (1998) Light-induced exposure of the cytoplasmic end of transmembrane helix seven in rhodopsin, *Proc. Natl. Acad. Sci. U.S.A. 95*, 12854−12859.
91. Choi, G., Landin, J., Galan, J. F., Birge, R. R., Albert, A. D., and Yeagle, P. L. (2002) Structural studies of metarhodopsin II, the activated form of the G-protein coupled receptor, rhodopsin, *Biochemistry 41*, 7318−7324.
92. Nikiforovich, G. V., and Marshall, G. R. (2003) Three-dimensional model for meta-II rhodopsin, an activated G-protein-coupled receptor, *Biochemistry 42*, 9110−9120.
93. Ruprecht, J. J., Mielke, T., Vogel, R., Villa, C., and Schertler, G. F. (2004) Electron crystallography reveals the structure of metarhodopsin I, *EMBO J. 23*, 3609−3620.

BI048413Q